sustainability

MDPI

Article

Decentralized Control of DC Microgrid Based on Droop and Voltage Controls with Electricity Price Consideration

Al Faris Habibullah, Faris Adnan Padhilah and Kyeong-Hwa Kim *

Research Center for Electrical and Information Technology, Department of Electrical and Information Engineering, Seoul National University of Science and Technology, 232 Gongneung-ro, Nowon-gu, Seoul 01811, Korea; al.faris.habibullah@gmail.com (A.F.H.); farisap.fa@gmail.com (F.A.P.)
* Correspondence: k2h1@seoultech.ac.kr; Tel.: +82-2-970-6406

Abstract: In this paper, a power flow control strategy (PFCS) for the decentralized control of DC microgrids (DCMGs) is proposed to enhance the flexibility and scalability of the microgrid power system. The proposed scheme is achieved by combining the droop control and DC-link voltage control with the consideration of the electricity price condition. Generally, the droop control method can be used effectively in decentralized DCMGs to achieve power-sharing without additional communication links. However, the deviation of the DC-link voltage caused by the droop control affects the amount of power delivered to the load. As an alternative, the DC-link voltage control can be used to prevent such a deviation. To combine both control schemes in this study, the utility grid (UG) unit uses the DC-link voltage control to exchange the power between the DC-link and a UG in the grid-connected mode, while a distributed generator (DG) and energy storage system (ESS) units use the droop control method in the islanded mode. The operating modes of the UG, DG, ESS, and load units are determined by the deviation values of the DC-link voltage to maintain DCMG power balance. The overall PFCS is also developed for a decentralized DCMG system by taking into consideration several uncertainties such as DG power variation, battery state of charge (SOC) level, load demand, and grid availability. The proposed PFCS also considers electricity price conditions to adaptively change the DC-link voltage level for the purpose of minimizing the utility cost. When the DC-link voltage level is reduced due to the high electricity price condition, the proposed droop controller is designed such that the ESS unit operates with a discharging mode, which leads to the required minimum power support from the UG. The effectiveness of the proposed PFCS is demonstrated by comprehensive simulation and experimental results under various conditions. Those test results clearly confirm the control flexibility and overall performance of the proposed PFCS for a decentralized DCMG system.

Keywords: DC microgrid; DC-link voltage control; decentralized control architecture; droop control; electricity price consideration; power flow control

Citation: Habibullah, A.F.; Padhilah, F.A.; Kim, K.-H. Decentralized Control of DC Microgrid Based on Droop and Voltage Controls with Electricity Price Consideration. *Sustainability* **2021**, *13*, 11398. https://doi.org/10.3390/su132011398

Academic Editors: Luis Carlos Herrero de Lucas, Dionisio Ramírez Prieto and Nestor Francisco Guerrero Rodriguez

Received: 1 September 2021
Accepted: 12 October 2021
Published: 15 October 2021

1. Introduction

The increase of electronic devices has triggered the growth of research in electrical power systems, especially in renewable energy sources (RESs) like wind and solar resources. Several RES units are connected into electrical power systems as distributed generators (DGs) [1]. RES-based DGs are commonly interconnected with an energy storage system (ESS) to enhance the power system flexibility by storing the surplus power from DG and using it when necessary. On the other hand, the direct interconnection of ESSs and DGs in a utility grid (UG) supply leads to several control-related issues associated with different frequencies and voltages [2]. As a result, the microgrid concept has been introduced to develop an effective integration of power units such as the AC grid, DGs, and ESSs, and loads through a power converter interface in an electrical power system [3].

A microgrid uses a bus bar as the point of common coupling (PCC) which is used to connect power units and to share the power among electrical power sources [4]. According

to the type of bus voltage, the microgrid is classified as DC microgrids (DCMGs), AC microgrids (ACMGs), and hybrid AC-DC microgrids (AC-DCMGs) [5]. Even though most conventional UGs use AC power systems, the concept of the DCMG has become popular due to several benefits, such as the absence of harmonics, frequencies, and reactive power issues [6]. Moreover, the DCMG is more advantageous than the ACMG in view of efficiency, reliability, and stability [7]. As a result, the DCMG system has gotten a lot of attention in recent microgrid research.

According to grid availability, the microgrid operation is also divided into the grid-connected mode and islanded mode [8]. In the grid-connected mode, the power balance of the microgrid system is primarily maintained and supported by the UG. On the other hand, in the islanded mode, the microgrid power balance is ensured by a coordinated operation of only the power units such as DGs and ESSs.

In the grid-connected mode, there have been concerns about optimizing the power consumption cost of a microgrid because the power injected into or absorbed from the UG commonly affects the electricity cost. Real-time pricing (RTP), time-of-use (TOU) pricing, and stepwise-power-tariff (SPT) pricing are commonly used electricity pricing methods in residential use [9]. The TOU pricing divides a day into peak-valley and peak-normal-valley periods [10]. The RTP system also divides a day into high-cost and low-cost periods with greater variation than that in the TOU pricing [11]. On the other hand, the SPT method divides the monthly electricity into several levels based on monthly electricity use for the purpose of restraining the overconsumption of electricity [12]. Based on the electricity pricing method, a DCMG system can be designed to minimize electricity consumption.

Selecting an appropriate coordinated control architecture for a DCMG system is very important since it might impact the reliability and flexibility of a DCMG as well as the minimization of electricity consumption. In view of the communication perspective, the coordinated control architecture of a DCMG can be classified into three groups: centralized control, distributed control, and decentralized control [13]. In a centralized control, all power units communicate with the central controller through digital communication links (DCLs). Based on the data collected and processed from each power unit, the central controller determines the operating modes of each power unit [14,15]. The distributed control also employs DCLs to connect each power unit. However, contrary to the centralized control, the power units are only connected with adjacent neighbors by DCLs. In the distributed control, each power unit determines its operating mode independently based on the data collected from its surroundings [15,16]. On the other hand, under decentralized control, each power unit decides its operating mode without using DCLs [17–19]. The absence of the DCLs is a substantial advantage of this control scheme because the problem caused by the communication delay does not exist. Furthermore, the system installation is much easier and more efficient, which enhances the microgrid system scalability and flexibility significantly.

The decentralized control scheme operates without additional communication lines. Instead, this scheme mainly relies on local measurements to realize the desired operating modes of the power unit. In general, the DC-link voltage is commonly used in the decentralized control method as an indicator to determine the operating modes of each power unit. For instance, surplus power within a DCMG increases the DC-link voltage, whereas a deficit power reduces it. Additionally, if the DC-link voltage decreases, it implies that the power injected into the DCMG is less than the required power demand [20]. Based on the behavior of the DC-link voltage, voltage-based droop control methods have been presented for power-sharing among power sources [21]. This scheme implements a virtual resistor to control each converter in a microgrid system. Voltage/current (V/I) or voltage/power (V/P) droop control schemes are the common methods used for decentralized control of a DCMG [22].

Several power flow control strategies (PFCSs) based on a decentralized control approach with droop control have been presented to ensure the system power balance under various conditions [23–25]. In [23], mode-adaptive decentralized control for a renewable

DCMG composed of DG, ESS, UG, and load demand is proposed to achieve power-sharing without any communication link. In this scheme, according to the DC-link voltage levels of the DCMG, the entire system operation is divided into three modes, namely, utility dominating, storage dominating, and generation dominating. The study in [24] presents a PFCS in an islanded DCMG integrated with a photovoltaic (PV), battery, and hydrogen system by using the mode-triggered droop method. Even though this study presents the integration of hydrogen and a battery into a DCMG, as well as presents a control scheme based on three battery state of charge (SOC) conditions, the study only deals with an islanded DCMG operation. To overcome such an issue, this study classifies the operating modes into eight based on six DC-link voltage levels which are defined considering the PV power, load demand, and SOC levels of the battery and hydrogen system. A different PFCS is developed in [25] for the DCMG composition similar to the study in [23]. In [26], a coordinated control operation of the DCMG is determined by using droop control based on integrator current sharing. This study also introduces a load shedding scheme in the PFCS to sustain the power balance in case the loads are too heavy.

In spite of the good power-sharing characteristic of the droop control, the deviation of the DC-link voltage V_{dc} is a disadvantage of this control method. The significant deviation of the DC-link voltage affects the amount of power delivered into the load. In contrast, the slight deviation may affect the accuracy of the power-sharing. As an alternative, the DC-link voltage control scheme can be used to regulate V_{dc} to a constant value by injecting power into the microgrid DC-link, or absorbing the power from it [26]. In [27,28], the DC-link voltage controller successfully achieves optimal power-sharing in the centralized and distributed control approaches, respectively. In the PFCSs of both studies, to achieve power-sharing by the DC-link voltage controller, it should be implemented by at least one power unit in every operation mode of a DCMG.

To enhance the flexibility and scalability of the microgrid system, this paper presents a PFCS for the decentralized control of a DCMG, which combines the droop control and DC-link voltage control with consideration of the electricity price condition. The DCMG system considered in this study consists of a UG, ESS, DG, and load units. By using the proposed scheme, each power unit effectively decides its operating mode without using DCLs like the conventional decentralized control. By using the combined control method for DCMG, the UG unit uses the DC-link voltage control to exchange the power between the DC-link and UG in the grid-connected mode, while the DG and ESS units use the droop control method in the islanded mode. As a result, the deviation of V_{dc} can be avoided in the grid-connected mode since the DC-link voltage control scheme regulates V_{dc} to a constant value. The overall PFCS is developed for the given decentralized DCMG system by taking into consideration the DG generation power, battery SOC level, grid availability, load demand, and electricity price condition. The operating modes of all power units are autonomously determined according to the deviation values of the DC-link voltage to maintain the DCMG power balance. Furthermore, the proposed PFCS adaptively changes the DC-link voltage level according to electricity price conditions to minimize the utility cost.

The simulation is conducted to verify the effectiveness of the proposed decentralized control scheme by using the Powersim (PSIM) software (9.1, Powersim, Rockville, MD, USA) under two different levels of SOC, two grid conditions, and two electricity price conditions. The simulation results validate that the proposed scheme can effectively achieve optimal power-sharing even under various conditions such as the abrupt transition of DG generation power, uncertain battery SOC level, grid availability, load demand, and electricity price change. The experimental results are also presented to support the simulation results by using a prototype DCMG system. The main contributions of this paper are as follows:

(i) The proposed decentralized DCMG system can achieve power-sharing and energy management among power units without using additional communication links. In the grid-connected mode, power-sharing and energy management are ensured by

the UG considering the electricity price condition. On the contrary, in the islanded mode, they are achieved by the DG, ESS, and load units according to the wind power, battery SOC, and load demand condition.

(ii) A PFCS for a decentralized DCMG architecture that combines voltage droop control and DC-link voltage control is proposed. The proposed PFCS consisting of eleven operating modes enhances the DCMG system reliability in the presence of uncertainties such as the wind power variation, battery SOC level, load demand, and grid availability. In addition, the proposed droop control can be implemented easily in various power sources like DG and ESS, which enhances the microgrid system scalability more flexibly.

(iii) Depending on the electricity price condition, the proposed PFCS adaptively changes the DC-link voltage level in the grid-connected mode to minimize the utility cost without affecting the DCMG system operation stability. Hence, by reducing the DC-link voltage level during a high electricity price condition, the UG supports only the required minimum power to DCMG, or, conversely, the UG absorbs the maximum power available from DCMG.

This paper is organized as follows: A configuration of DCMG considered in this study is described in Section 2. Section 3 presents the proposed decentralized control strategy of DCMG including the operating mode definition, PFCS, and control block diagram of each power system in detail. The simulation and experimental results are demonstrated under various operating conditions in Sections 4 and 5. Finally, the conclusion of the paper is given in Section 6.

2. Configuration of the DCMG

The configuration of the DCMG studied in this paper, as shown in Figure 1, consists of four main power units: a wind turbine unit as a DG, a battery unit as an ESS, a UG unit to connect the DCMG with the UG, and a load unit to represent load demand. Power units are connected to the DC-link of the DCMG to exchange the power through different converter topologies and control strategies. The UG power unit and battery unit operate in a bidirectional way with bidirectional power flow, which can inject the power into DC-link or absorb the power from DC-Link. In contrast, the wind turbine power unit and the load unit operate only in a unidirectional manner with unidirectional power flow. Whereas the wind turbine unit only injects the power into the DC-link, the load unit only absorbs the power from the DC-link.

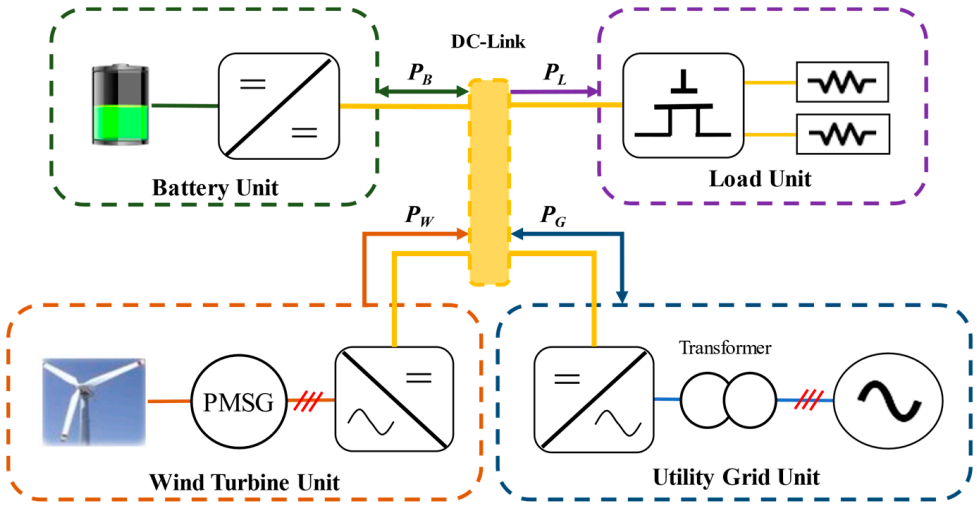

Figure 1. Configuration of DCMG.

Figure 1 also shows bidirectional or unidirectional power flows between the DC-link and each power unit, in which P_B denotes the power flow between the DC-link and battery

unit, P_L denotes the power flow between the DC-link and load unit, P_W denotes the power flow between the DC-link and wind turbine unit, and P_G denotes the power flow between the DC-link and UG unit, respectively. For simulation and experimental verification, the reference direction of the current and power flow is defined. In the DC-link, when the power is injected and the current flows into the DC-link, those variables are denoted as negative (−). On the contrary, when the power is absorbed from and the current flows out of the DC-link, those variables are denoted as positive (+).

The UG power unit connects the main grid into the DC-link by using a transformer and a bidirectional AC/DC converter. In the wind turbine power unit, a permanent magnet synchronous generator (PMSG) converts the mechanical output power into the electrical power that is delivered into the DC-link through a unidirectional AC/DC converter. The battery power unit uses a bidirectional interleaved DC/DC converter to exchange the power between the battery and DC-link. Finally, in the load unit, the electronic switches are installed to implement load shedding or reconnection. The detailed operations and control methods of converters are determined by the proposed PFCS of DCMG and are described in subsequent sections.

3. Proposed Decentralized Control Strategy of DCMG

3.1. Operating Mode Definition of DCMG

As mentioned before, the DC-link voltage V_{dc} can be used to determine the operating modes of each power unit in the decentralized DCMG control. To realize the proposed control scheme, the DC-link voltage reference should be set in the grid-connected mode as well as the islanded mode. In the grid-connected mode, the V_{dc} reference is chosen according to the electricity price condition. In the islanded mode, the V_{dc} reference should be selected in accordance with the voltage range based on the proposed power-sharing strategy. Figure 2 shows the operating mode definition of power units according to the V_{dc} values in the grid-connected mode and the islanded mode.

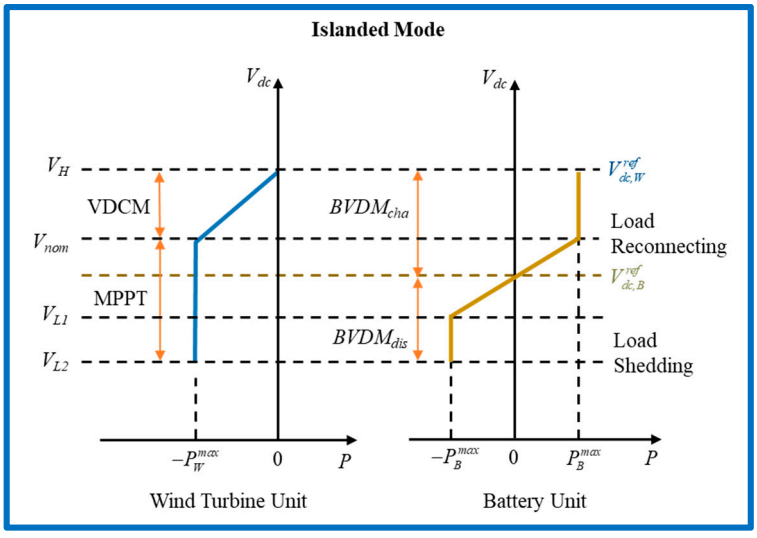

(**a**)

Figure 2. *Cont.*

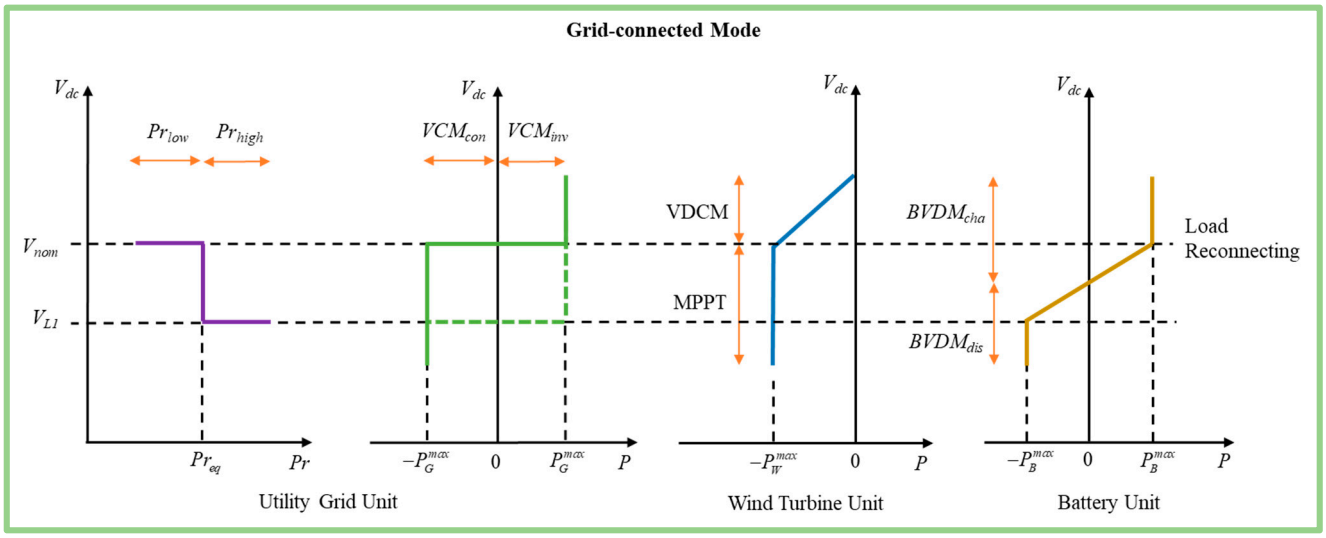

(**b**)

Figure 2. Operating mode definition of power units in grid-connected mode and islanded mode. (**a**) Islanded mode; (**b**) Grid-connected mode.

Since the UG is not connected to the DCMG system in the islanded mode, the UG cannot supply the power even in the circumstance of a power deficit in the DCMG system. Conversely, the UG cannot absorb surplus power from the DCMG system. As a result, the main purpose of the microgrid system in the islanded mode is to supply local loads reliably without grid support. In the islanded mode, the DC-link voltage V_{dc} is regulated either by wind turbine unit or by battery unit based on the droop control according to the V_{dc} deviation to determine the operating modes of each unit. The proposed droop control works with four voltage levels in the islanded mode, that is, the maximum voltage (V_H), the nominal voltage (V_{nom}), the level 1 minimum voltage (V_{L1}), and the level 2 minimum voltage (V_{L2}). The following conditions are formulated to determine the operating modes of each power unit based on V_{dc} value:

- In the case of $V_{nom} < V_{dc} < V_H$: The wind turbine unit produces power more than the sum power needed for the load demand P_L and the maximum battery charging P_B^{max}. As a result, the DCMG system has surplus power, which causes V_{dc} to increase beyond the nominal value V_{nom}. To prevent the DCMG system from overvoltage caused by surplus power, the wind turbine unit operates with the voltage droop control mode (VDCM), in this case to regulate V_{dc} by adjusting its power generation. Meanwhile, the battery unit uses the battery voltage droop control by charging mode ($BVDM_{cha}$).
- In the case of $V_{L2} < V_{dc} < V_{nom}$: The wind turbine unit operates in the maximum power point tracking (MPPT) mode to draw the maximum power P_W^{max}. However, the generation power is not sufficient to supply the sum power for P_L and P_B^{max}, which leads to V_{dc} regulation below the value V_{nom}. In this condition, depending on the wind power injected into the DCMG system, the battery unit automatically regulates V_{dc} during the charging operation with battery voltage droop control by charging mode ($BVDM_{cha}$), or during the discharging operation with battery voltage droop control by discharging mode ($BVDM_{dis}$). In this condition, the battery unit automatically regulates V_{dc} according to the DCMG power relation. If P_W^{max} by the wind turbine unit is larger than P_L, V_{dc} is regulated to the region between V_{nom} and $V_{dc,B}^{ref}$. Then, the remaining power is absorbed by the battery unit which operates with the battery voltage droop control by charging mode ($BVDM_{cha}$). Otherwise, if P_W^{max} is less than P_L, V_{dc} is regulated to the region between $V_{dc,B}^{ref}$ and V_{L1}. Then, additional power should be supplied to load by the battery unit by operating with the battery voltage droop control by discharging mode ($BVDM_{dis}$).

- In the case of $V_{dc} < V_{L2}$: If the DC-link voltage V_{dc} is further reduced below the level 2 minimum voltage V_{L2}, load shedding should be used by the load management system as a final solution to prevent the DCMG system from collapsing in this critical situation. By combining the algorithm from [25,28], load shedding is automatically activated when V_{dc} reaches to V_{L2} based on the load priority in this study. On the other hand, when the system is back to normal, the load reconnecting algorithm is executed to connect the disconnected load to improve the reliability of the DCMG system. In this paper, the load reconnecting algorithm automatically starts when V_{dc} is recovered to V_{nom} according to the load priority.

In the grid-connected mode, the DC-link voltage, V_{dc}, is regulated to a constant value by the UG unit by using the DC-link voltage control. The UG injects the power to the DC-link or absorbs the power from the DC-link. Considering the electricity price condition, two voltage values of V_{nom} and V_{L1} are adaptively chosen for the DC-link voltage level in the grid-connected mode to reduce the use of power from the UG or to increase the injected power into the UG under a high electricity price condition. In the grid-connected mode, the operations of DG and battery units are the same as those in the islanded mode.

- In the case of a low electricity price condition (Pr_{low}): In this condition, the UG unit regulates V_{dc} to V_{nom} value, the battery unit operates with $BVDM_{cha}$ to charge the battery with the maximum battery charging power P_B^{max}, and the wind turbine operates in the MPPT mode. The operating mode of the UG unit is dependent on P_W, P_B^{max}, and P_L as well as the battery SOC level. If P_W is more than the sum of P_L and P_B^{max}, the surplus power is absorbed by the UG by using DC-link voltage control by the inverter mode (VCM_{inv}) operation. Otherwise, if P_W is less than the sum of P_L and P_B^{max}, the UG injects the power into DCMG by using the DC-link voltage control by the converter mode (VCM_{con}) operation.
- In the case of a high electricity price condition (Pr_{high}) : In this condition, the UG unit regulates V_{dc} to the V_{L1} value, the wind turbine unit operates in the MPPT mode, and the battery unit operates with $BVDM_{dis}$ to supply the maximum battery discharging power P_B^{max} into the DCMG. The operating mode of the UG unit is dependent on P_W, P_B^{max}, and P_L as well as the battery SOC level. If the wind turbine and battery units can provide more power than the demand load, the remaining power is absorbed into the UG by operating the UG with the VCM_{inv} operation. Otherwise, if the sum of P_W and P_B^{max} is less than P_L, or, if the batter has the critical SOC level, the UG unit injects the power into DCMG through the VCM_{con} operation.

Table 1 shows the definition of the operating modes for each power unit in the proposed decentralized DCMG.

Table 1. Operating mode definition of power units in the proposed PFCS for a decentralized DCMG.

Power Unit	Description	Operating Modes
Utility grid (UG) unit	The UG unit is disconnected due to fault	Fault
	DC-link voltage control by inverter mode	VCM_{inv}
	DC-link voltage control by converter mode	VCM_{con}
Battery unit	Idle mode	IDLE
	Battery voltage droop control by discharging mode	$BVDM_{dis}$
	Battery voltage droop control by charging mode	$BVDM_{cha}$
Wind turbine unit	Maximum power point tracking mode	MPPT
	Voltage droop control mode	VDCM
Load unit	Load shedding	SHED
	Load reconnecting	Reconnection
	Load in normal condition	Normal

3.2. Power Flow Control of DCMG

In this section, the proposed PFCS is explained for decentralized control of the DCMG. The proposed PFCS determines the operating modes of all the power units in the DCMG considering the wind power generation, load demand, battery SOC state, and UG availability. Moreover, the electricity price condition is also considered in the grid-connected mode to decide the operation of the power units. Power electronics interfaces shown in Figure 1 are controlled to realize the selected operation of the power units.

Figure 3 shows the proposed PFCS for decentralized control of the DCMG, which is composed of eleven operating modes. Operating modes 1, 2, 9, 10, and 11 represent the islanded mode, while operating modes three through eight represent the grid-connected mode, as depicted at the bottom of Figure 3. The detailed operations of the individual power units in each mode are shown in Table 2. The conditions and operations of DCMG power units corresponding to the eleven operating modes in Figure 3 and Table 2 are explained in detail as follows:

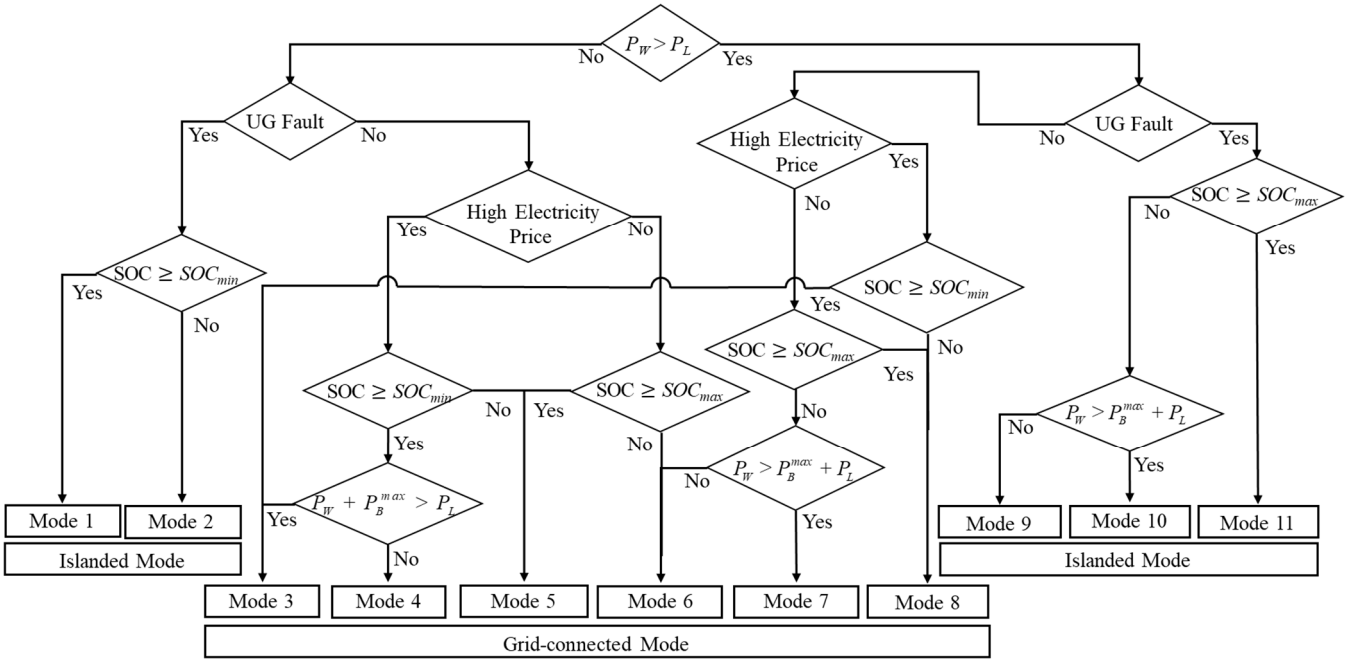

Figure 3. Proposed PFCS for decentralized control of DCMG.

Table 2. Operations of each power unit in the proposed PFCS.

Mode	Wind Power Agent	Grid Agent	Battery Agent	Load Agent
Mode 1	MPPT	Fault	IDLE	SHED
Mode 2	MPPT	Fault	$BVDM_{dis}$	Normal/SHED
Mode 3	MPPT	VCM_{inv}	$BVDM_{dis}$	Normal
Mode 4	MPPT	VCM_{con}	$BVDM_{dis}$	Normal
Mode 5	MPPT	VCM_{con}	IDLE	Normal/Reconnection
Mode 6	MPPT	VCM_{con}	$BVDM_{cha}$	Normal/Reconnection
Mode 7	MPPT	VCM_{inv}	$BVDM_{cha}$	Normal/Reconnection
Mode 8	MPPT	VCM_{inv}	IDLE	Normal/Reconnection
Mode 9	MPPT	Fault	$BVDM_{cha}$	Normal
Mode 10	VDCM	Fault	$BVDM_{cha}$	Normal/Reconnection
Mode 11	VDCM	Fault	IDLE	Normal/Reconnection

Operating mode one: In this mode, the DCMG system operates in the islanded mode because of the UG fault. Although the wind turbine unit injects the produced maximum power into the DC-link by the MPPT mode, the wind power is not sufficient to supply

the load demand. Furthermore, since the battery is in the minimum SOC level (SOC_{min}), the battery unit operates in the IDLE state. The power shortage in the DCMG system causes V_{dc} to decrease to the level 2 minimum voltage V_{L2} in Figure 2a, which initiates the load shedding to prevent the system from collapsing in this critical circumstance by disconnecting some less critical loads. If V_{dc} increases as a result of load shedding (this indicates that the wind power is slightly larger than the load demand), the operating mode is changed again into mode nine to charge the battery with the remaining power.

Operating mode two: This mode also represents the islanded DCMG operation under the UG fault and has similar conditions as the operating mode one. The only difference is that the battery SOC is higher than SOC_{min}. As a result, the battery unit can operate in $BVDM_{dis}$ to support additional power to the DCMG system based on the deviation level of V_{dc}. However, if the V_{dc} value is still decreasing even with the battery $BVDM_{dis}$ operation, this indicates that the load demand is larger than the supply power by the wind turbine and battery units. Finally, when V_{dc} reaches V_{L2}, the load shedding is automatically activated to protect the DCMG system. After the load shedding, if V_{dc} increases to $V_{dc,B}^{ref}$, the operating mode is changed to mode nine. Otherwise, operating mode two is still maintained.

Operating mode three: This mode occurs when the DCMG is connected to the UG under a high electricity price condition and when the battery SOC is higher than SOC_{min}. The wind turbine unit still uses the MPPT mode to inject the maximum power into the DC-link. As shown in Figure 2b, the UG unit selects V_{L1} for the V_{dc} level to minimize the utility power usage with a high electricity price condition. With V_{L1} value, the battery unit automatically changes its operation into $BVDM_{dis}$ with the maximum power, which causes additional power injection into the DCMG. Since the sum of battery and wind power which is supplied into DCMG exceeds the load demand, the remaining power will be supplied into the UG which operates in VCM_{inv}.

Operating mode four: Similar to operating mode three, this mode occurs when the DCMG is connected with the UG under a high electricity price condition and the battery SOC is higher than SOC_{min}. However, contrary to mode three, the load demand is still larger than the amount of maximum power from the battery and wind turbine which operate in $BVDM_{dis}$ and MPPT mode, respectively. As a result, the power shortage is absorbed from UG by operating in VCM_{con} in spite of the high electricity price condition.

Operating mode five: In the grid-connected mode of a high electricity price condition, the battery unit should discharge the power if possible to minimize utility power usage. However, if the battery has SOC_{min}, the battery unit is not able to intervene in the power exchange.

On the other hand, in the grid-connected mode with a low electricity price condition, the battery unit should absorb the power if possible to keep the battery with the maximum SOC level (SOC_{max}). However, if the battery already has SOC_{max}, the battery unit cannot exchange the power by charging operation. In the above two cases, the battery unit operates in the IDLE state without participating in the power exchange. The wind turbine unit still operates in the MPPT mode. The power deficit is provided by UG unit through the VCM_{con} operation.

Operating mode six: This mode occurs when the DCMG is connected with the UG while there is a low electricity price condition, and while the battery SOC is less than SOC_{max}. Since it is desirable to maintain the battery in SOC_{max} with a low electricity price condition, the battery unit works with $BVDM_{cha}$ operation. In this case, the wind power unit operates in the MPPT mode. Since the wind power is not sufficient for load demand and battery charging and the electricity price condition is low, the UG operates in VCM_{con}, and V_{dc} is regulated to V_{nom} value, according to Figure 2b.

Operating mode seven: This mode occurs when the DCMG is connected into the UG with a low electricity price condition and when the battery SOC is less than SOC_{max}. If the wind power can supply both the load demand and the maximum charging power of the battery, then the surplus power of the DCMG system is absorbed by the UG with VCM_{inv}

operation of the UG unit. In this case, the wind turbine unit works in the MPPT mode and the battery unit in $BVDM_{cha}$.

Operating mode eight: If the SOC condition of the battery unit reaches SOC_{max} in operating mode six or seven with the condition of $P_W > P_L$, the operating mode eight is activated. Also, this operating mode occurs when the battery unit reaches SOC_{min} with the condition of $P_W > P_L$ and a high electricity price. In this condition, the battery unit is in IDLE state to prevent the battery from overcharging. The wind turbine unit still operates in the MPPT mode. The remaining power in DCMG is injected into UG with VCM_{inv} operation of the UG unit.

Operating mode nine: This mode occurs in the islanded DCMG caused by a UG fault when the wind power generation is more than the load demand, but it is less than the sum of the load demand and the maximum battery charging power. In this condition, the wind turbine unit operates in the MPPT mode to supply the load. The remaining power is absorbed by the battery unit which regulates the DC-link voltage by the voltage droop control with $BVDM_{cha}$.

Operating mode 10: This mode occurs in similar conditions to operating mode nine, with only one difference, that the wind power generation is more than sum of the load demand and the maximum battery charging power. Due to increased power injection into the DC-link, V_{dc} is also increased beyond V_{nom}, which triggers an operation transition of the wind turbine unit from the MPPT mode into the voltage droop control mode (VDCM). Based on this control, the wind power unit adjusts the power generation from the wind turbine to regulate V_{dc}. The battery unit still operates in $BVDM_{cha}$.

Operating mode 11: If the battery is already in a fully charged state with SOC_{max} in operating mode nine or 10, this mode is selected. Since the battery unit is not capable of absorbing excessive power, its operation is changed into IDLE mode. The wind turbine unit still works in VDCM to adjust the wind power generation according to the load demand.

3.3. Control Implementation of Converters

In the decentralized DCMG control, the overall performance, operational reliability of the PFCS, and coordinated operating mode selection crucially depend on the control of converters in each power unit. In this Section, converter control techniques to implement the proposed PFCS for a decentralized DCMG are explicitly explained in detail. In this study, a bidirectional AC/DC converter, a unidirectional AC/DC converter, and an interleaved bidirectional buck-boost DC/DC converter are employed for the interface with the UG unit, wind turbine unit, and battery unit, respectively. The operating principles and control techniques of the converter are different for various types of converters. Figure 4 shows the control block diagram of converters to implement the control functions of each power unit as listed in Table 1. For converter control, all power units use cascaded loops, in which a voltage control is implemented as the outer loop, and a current control as the inner loop.

Figure 4a presents the control block diagram of a bidirectional AC/DC converter for the UG unit. As shown in Table 1, the UG should work in three operating modes, which are Fault, VCM_{con}, and VCM_{inv}. In the operating modes VCM_{con} and VCM_{inv}, the UG unit uses the proportional integral (PI) controller for the outer loop voltage control with the DC-link voltage reference $V_{dc,G}^{ref}$, in which the subscript '*G*' denotes the variables in the UG unit, and the superscript '*ref*' denotes the reference quantities. The DC-link voltage reference $V_{dc,G}^{ref}$ is selected based on the electricity price condition as shown in Figure 2b. The Outer loop PI controller which regulates the DC-link voltage produces the current reference $I_{q,G}^{ref}$, in which the subscript '*q*' and '*d*' denote the *q*-axis and *d*-axis variables, respectively. The current reference is negative in VCM_{con} mode while it is positive in VCM_{inv} mode, according to the definition of current direction and power flow in Section 2. The limiters with the proper sign are located after the PI controllers to restrict the magnitude of the current reference. With the obtained current reference, the inner loop current control is designed to ensure zero steady-state tracking errors [27]. The phase lock loop (PLL) is also employed to obtain

the grid phase angle information from $V_{d,G}^{ref}$ and grid phase voltages $V_{abc,G}$. The current control output generates the inverter voltage reference, which is applied to control the bidirectional AC/DC converter by a space vector pulse width modulation (SVPWM) and grid phase angle from the PLL.

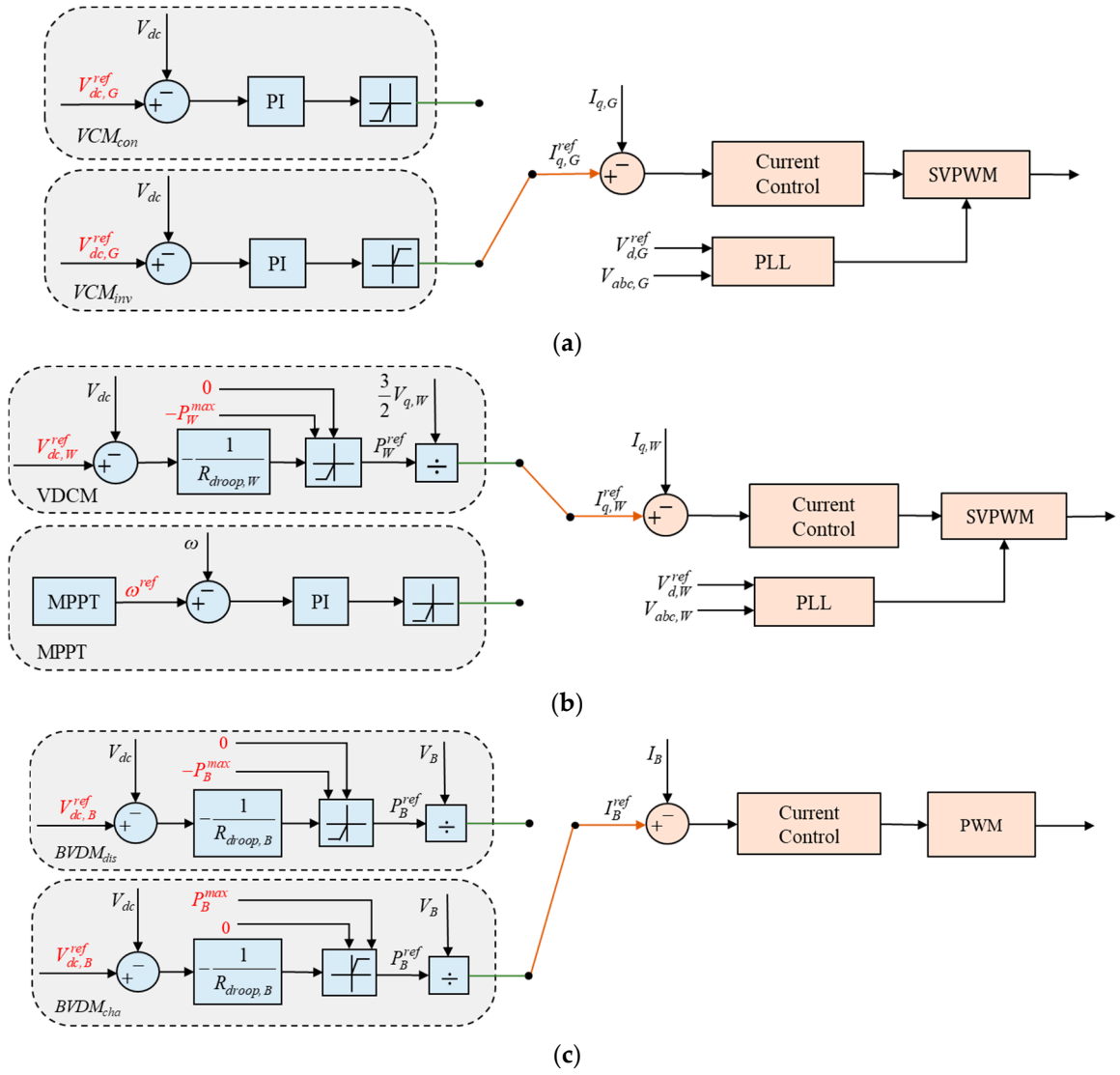

Figure 4. Control block diagram of converters. (**a**) Utility grid unit; (**b**) Wind turbine unit; (**c**) Battery unit.

Figure 4b shows the control block diagram of a unidirectional AC/DC converter for the wind turbine unit. The wind turbine unit should perform two operations, VDCM and MPPT, which are achieved by different outer loop controllers. However, the inner loop current control scheme has the same structure as the UG unit, as seen in Figure 4b. In Figure 4b, the subscript '*W*' denotes the variables in the wind turbine unit, and ω denotes the rotor angular speed. In the MPPT mode, the rotor angular speed to draw the maximum wind power is derived, and this value is used as the speed reference in the PI controller to generate the current reference of a unidirectional AC/DC converter. In VDCM, the current reference is generated from the DC-link voltage V_{dc} and the wind turbine voltage reference $V_{dc,W}^{ref}$ by using a voltage droop controller. To implement the voltage droop controller, $V_{dc,W}^{ref}$ should be determined first from the power and voltage relation in Figure 2 as follows:

$$V_{dc,W}^{ref} = V_{dc} - R_{droop,W} P_W \quad (1)$$

where $R_{droop,W}$ denotes the droop characteristic of the wind turbine unit in Figure 2 which is obtained as

$$R_{droop,W} = \frac{V_H - V_{nom}}{0 - (-P_W^{max})} = \frac{\Delta V_{dc}}{\Delta P_W}. \quad (2)$$

From (1) and (2), the power reference of the wind turbine unit P_W^{ref} is calculated for different values of V_{dc} as shown in Figure 4b. Then, this power reference is used to generate the current reference $I_{q,W}^{ref}$.

In Table 1, the battery unit should work in three operating modes, which are $BVDM_{cha}$, $BVDM_{dis}$, and IDLE. Figure 4c shows the control block diagram of a bidirectional buck-boost DC/DC converter for the operating modes $BVDM_{cha}$ and $BVDM_{dis}$, in which the subscript 'B' denotes the variables in the battery unit. As the outer loop controller, the battery unit uses a voltage droop control for these two modes to generate the current reference. To implement the voltage droop controller in the battery unit, the battery voltage reference $V_{dc,B}^{ref}$ is determined as follows:

$$V_{dc,B}^{ref} = V_{dc} - R_{droop,B} P_B \quad (3)$$

where $R_{droop,B}$ represents the droop characteristic of the battery unit in Figure 2 which can be obtained as follows:

$$R_{droop,B} = \frac{V_{nom} - V_{L1}}{P_B^{max} - (-P_B^{max})} = \frac{\Delta V_{dc}}{\Delta P_B}. \quad (4)$$

From (3) and (4), the power reference of the battery unit P_B^{ref} is calculated for different values of V_{dc}, as shown in Figure 4c. If the V_{dc} value is less than $V_{dc,B}^{ref}$, the battery power reference is negative, and vice versa. The negative power reference is dealt with by $BVDM_{dis}$, and the positive power reference by $BVDM_{cha}$. Then, the battery current reference is generated by dividing the power reference by the battery voltage. The inner loop current controller is designed with this current reference to produce the duty cycle d, which is fed to a pulse width modulation (PWM) block. The IDLE mode of the battery unit is realized by turning off the connection switch between the battery unit and the DCMG.

4. Simulation Results

To validate the overall control performance, operational reliability, and effectiveness of the proposed PFCS for a decentralized DCMG system, the simulations based on the PSIM software were carried out. The transient and steady-state performance of the proposed decentralized DCMG system were evaluated under several uncertainties, including the wind power generation, load demand, battery SOC status, grid connection, and electricity price condition. Table 3 shows the specification and parameters of the DCMG system used in the simulation. The simulation results are presented for three cases which are the high battery SOC case, low battery SOC case, and high electricity price case. The DC-link voltage is mainly controlled by the wind turbine unit in $V_{nom} < V_{dc} < V_H$ and by the battery unit in $V_{L2} < V_{dc} < V_{nom}$ in islanded mode. On the other hand, it is controlled by the UG unit to two constant values of V_{nom} and V_{L1} in grid-connected mode. In these simulation tests, P_W, P_G, P_L, and P_B denote the power of the wind turbine unit, UG unit, load unit, and battery unit, respectively, and the reference direction of current and power flow follows the definition in Section 2.

Table 3. Specification and parameters of DCMG system.

Power Units	Parameters	Symbol	Value
UG unit	Grid voltage	V_G^{rms}	220 V
	Grid frequency	f_G	60 Hz
	Transformer Y/Δ	T	380/220 V
	Inverter-side inductance of LCL filter	L_1	1.7 mH
	Parasitic resistance in L_1	R_1	0.5 Ω
	Grid-side inductance of LCL filter	L_2	1.7 mH
	Parasitic resistance in L_2	R_2	0.5 Ω
	Filter capacitance of LCL filter	C_f	4.5 µF
Wind turbine unit	PMSG stator resistance	R_S	0.64 Ω
	PMSG *dq*-axis inductance	L_{dq}	0.82 mH
	PMSG number of poles	p	6
	PMSG inertia	J	0.111 kgm^2
	PMSG flux linkage	ψ	0.18 Wb
	Converter filter inductance	L_W	7 mH
	Parasitic resistance in L_W	R_W	0.2 Ω
Battery unit	Maximum *SOC*	SOC_{max}	90%
	Minimum *SOC*	SOC_{min}	20%
	Rated capacity	C	30 Ah
	Maximum voltage	V_B^{max}	180 V
	Converter filter inductance L	L_B	7 mH
Load unit	Power of load 1	P_{L1}	200 W
	Power of load 2	P_{L2}	200 W
	Priority level: load 2 > load 1	-	-
DC-link	Nominal voltage	V_{nom}	400 V
	Maximum voltage	V_H	410 V
	Level 1 minimum voltage	V_{L1}	390 V
	Level 2 minimum voltage	V_{L2}	385 V
	Capacitance	C_{dc}	4 mF

4.1. High Battery SOC Case

Figure 5 shows the simulation result for the high battery SOC case when the DCMG operates in the grid-connected mode to emphasize the effectiveness of the DC-link voltage controller. In this case, the power balance is achieved by regulating the DC-link voltage V_{dc} to a constant value under the variation of the wind power generation, load demand, and uncertain battery SOC condition. The DC-link voltage is controlled by the UG unit all the time with V_{nom} (400 V) as the voltage reference.

In Figure 5, the DCMG system starts at t = 0.05 s in the grid-connected mode with the condition that the battery SOC is less than SOC_{max}, and the wind turbine unit generates less power than the sum of load demand P_L and the maximum battery charging power P_B^{max}. Then, the DCMG operates in operating mode six, in which the system power balance is guaranteed by the UG unit with VCM_{con}. Since V_{dc} is at the nominal value V_{nom}, the wind turbine unit works in the MPPT mode, the battery unit is in $BVDM_{cha}$ with P_B^{max}, and all loads are fed.

Once the wind power P_W is increased higher than the sum of the load demand P_L and P_B^{max} at t = 0.25 s, the UG unit changes the operating mode from VCM_{con} into VCM_{inv} to inject the surplus power into the UG. As a result, the DCMG operation changes to operating mode seven. At t = 0.5 s, the load demand P_L suddenly decreases, which increases the power absorbed by the UG. However, despite the injected power variation into the UG, the DC-link voltage is stably maintained to the nominal value as before.

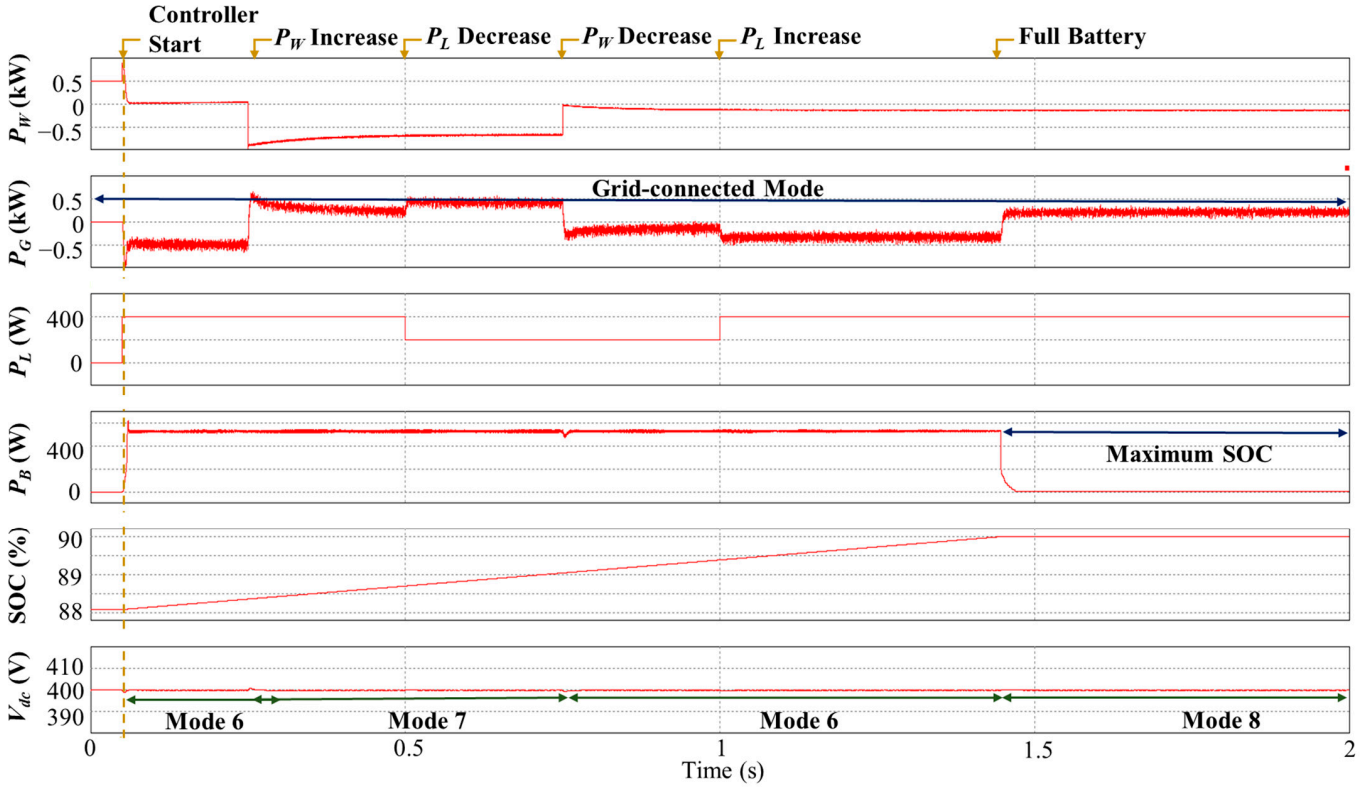

Figure 5. Simulation result of DCMG in grid-connected mode in the case of a high battery SOC level with P_W and P_L variations.

The operating mode seven lasts until t = 0.75 s when the wind power P_W suddenly decreases to a value less than the sum of P_L and P_B^{max}. This reduction causes the UG unit to change the operation from VCM_{inv} into VCM_{con}. Then, the DCMG operation is restored again to the operating mode six. Even when the load demand P_L is increased at t = 1.0 s, the DCMG operation is not changed. Only the power supplied by the UG is increased, and there is no noticeable difference in the DC-link voltage regulation performance.

Once the battery reaches a fully charged condition with SOC_{max} at t = 1.45 s, the battery unit automatically changes the operation from $BVDM_{cha}$ into IDLE to prevent the battery from overcharging. This causes surplus power in the DCMG system, which is absorbed by the UG by changing the UG operation from VCM_{con} to VCM_{inv}. As a result, the entire DCMG system changes the operating mode from six to eight.

From Figure 5, it is clear that the DC-link voltage controller effectively achieves the power balance in the grid-connected mode of a decentralized DCMG system under uncertainties of wind power generation, load demand, and battery SOC status.

To emphasize the flexibility of a droop controller that achieves the power balance, Figure 6 shows the simulation result for a high battery SOC case when the DCMG has a mode transition between the islanded mode and the grid-connected mode. Initially, the DCMG system starts in the islanded mode with a fully charged condition (SOC_{max}) of the battery and the wind power generation P_W is greater than the load demand P_L. In this case, the battery and UG units cannot absorb the surplus power. Since the decentralized control does not use any additional communication links to change the operating mode, the V_{dc} increase caused by surplus power in DCMG can be used effectively to shift the wind turbine unit operation into VDCM. In this condition, the wind turbine unit takes the role of the DC-link voltage regulation based on the voltage droop control to reduce the generation power. As a result, the DCMG operates in operating mode 11 and the DC-link voltage is regulated to a value slightly higher than V_{nom} due to the droop characteristic in Figure 2a.

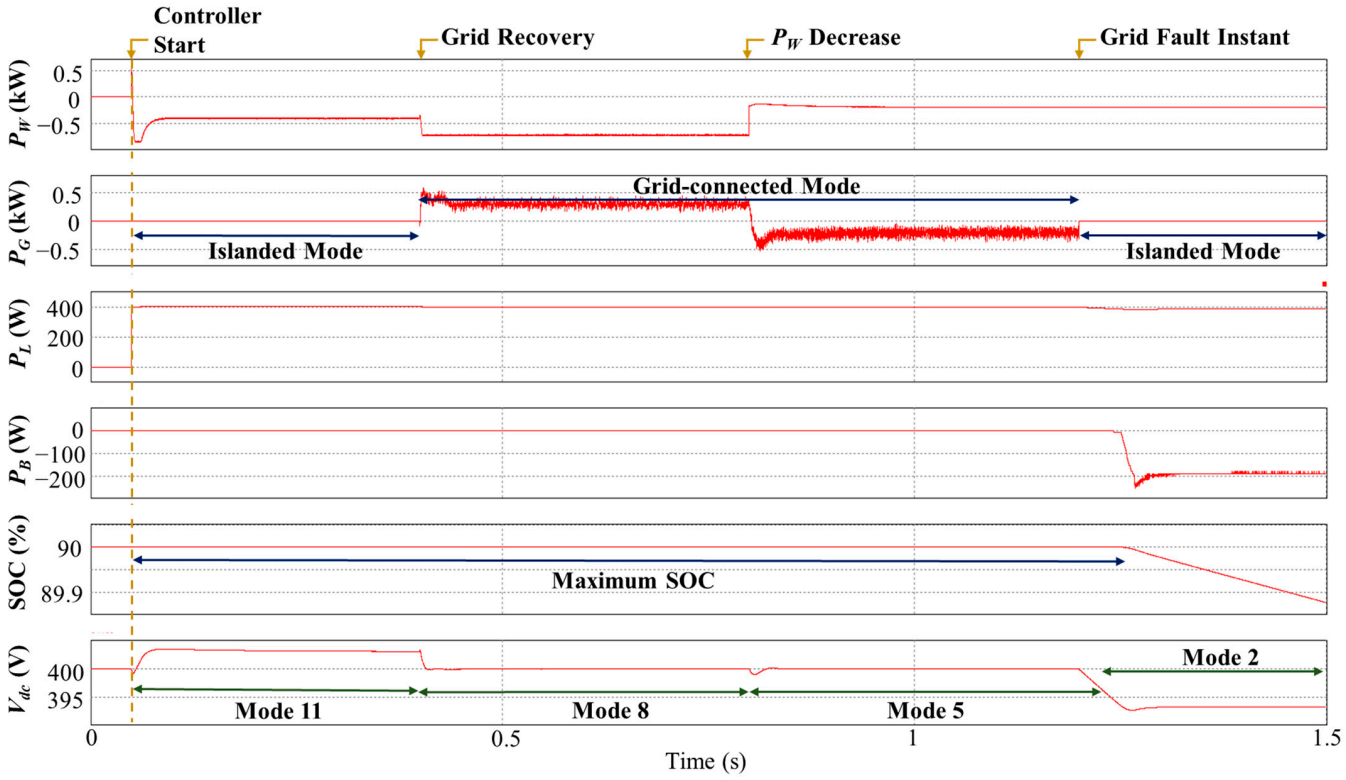

Figure 6. Simulation result of DCMG in the case of a high battery SOC level with a transition between islanded mode and grid-connected mode.

Once the UG is recovered from the fault at t = 0.4 s, the UG unit takes the control of the DC-link voltage with V_{nom}. Even though the battery is in a fully charged condition, the surplus power can still be absorbed by the UG unit. This causes the wind turbine unit operation to switch back to MPPT mode. In this case, the DCMG operates in operating mode eight, in which the UG unit ensures the system power balance by operating VCM_{inv}.

When, the wind power generation suddenly becomes less than the load demand P_L at t = 0.8 s, the UG unit changes the operation from VCM_{inv} into VCM_{con} to supply the power deficit, resulting in the DCMG operating mode changing from eight to five.

It is assumed that the system returns to the islanded mode due to the UG fault at t = 1.2 s. At this instant, because the wind power P_W is less than the load demand P_L, the battery unit automatically regulates the DC-link voltage V_{dc} by changing its operation from IDLE to $BVDM_{dis}$, which causes the DCMG operating mode to change from five to two. According to the voltage droop control characteristic in Figure 2a, the DC-link voltage level is maintained lower than V_{nom}.

Figure 6 also confirms the flexibility and overall performance of the proposed PFCS and droop control strategy to achieve the power balance in the decentralized DCMG system even when the DCMG experiences a mode transition between the islanded mode and grid-connected mode.

4.2. Low Battery SOC Case

To demonstrate the reliability of the proposed PFCS and droop control strategy, Figure 7 shows the simulation result in the case of a low battery SOC level under the transition between the islanded mode and grid-connected mode.

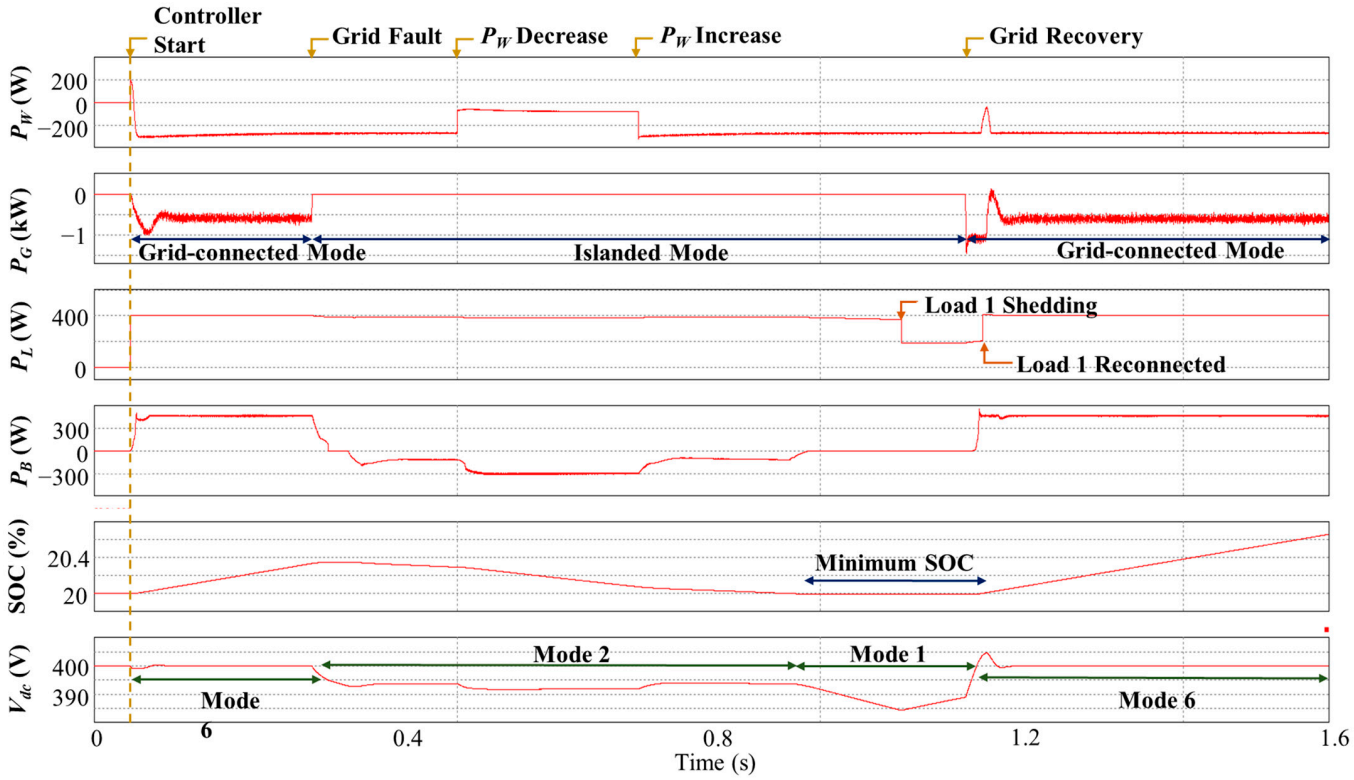

Figure 7. Simulation result in the case of a low battery SOC level with transition between islanded mode and grid-connected mode.

The DCMG system starts at t = 0.05 s in the grid-connected mode with the condition that the battery SOC is less than SOC_{max} and P_W is less than the sum of load demand P_L and the maximum battery charging power P_B^{max}. In this case, the DCMG operates in operating mode six before the grid fault occurs at t = 0.27 s.

In the islanded mode due to the UG fault, since P_W is less than the sum of P_L and P_B^{max}, the DC-link voltage V_{dc} decreases from V_{nom} toward V_{L1}, which triggers the battery unit operation change from $BVDM_{cha}$ into $BVDM_{dis}$. Then, the DCMG changes its operation from operating mode six to two. Even when P_W is reduced at t = 0.5 s, the DCMG remains in this operating mode. As P_W is reduced, the DC-link voltage also decreases, which causes the battery unit to supply more power to the DC-link. When P_W is increased again to the previous level at t = 0.7 s, the DC-link voltage level and the battery discharging power are returned to the values before t = 0.5 s.

Once the battery SOC reaches SOC_{min} at t = 0.94 s, the battery unit stops discharging by changing the operation from $BVDM_{dis}$ into IDLE. Due to the power deficit in the DCMG, the DC-link voltage gradually decreases to the V_{L2} level as shown in Figure 2a. With this level of the DC-link voltage, the load shedding algorithm is automatically activated to disconnect loads with the lowest priority. This mode corresponds to the operating mode one in Figure 3. As a result of the load shedding process, it is shown that the DC-link voltage is increasing because P_W is larger than P_L.

As the UG is recovered at t = 1.1 s, the DCMG system returns to the grid-connected mode, and the UG unit immediately starts the control of the DC-link voltage to V_{nom} by the operating mode VCM_{con}. As soon as the DC-link voltage approaches V_{nom}, the load reconnecting algorithm is triggered to reconnect the load which was disconnected. At the same time, the battery is charged with $BVDM_{cha}$. This mode corresponds to operating mode six.

This simulation result also confirms a reliable decentralized DCMG system operation and load management even in the presence of mode transition between the islanded mode and grid-connected mode.

Figure 8 shows the behavior of the DC-link voltage in the islanded mode to demonstrate the performance and reliability of the voltage droop control and load management.

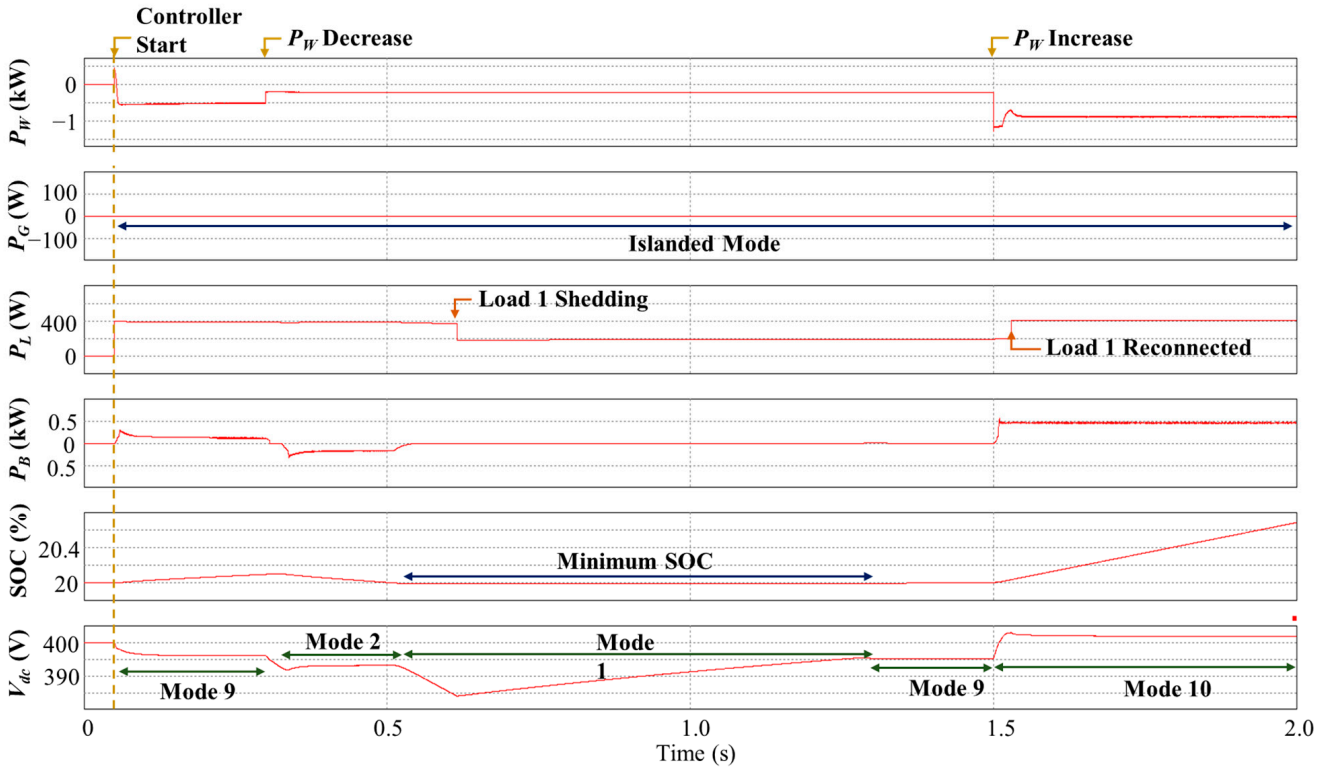

Figure 8. Simulation result in the case of a low battery SOC level with P_W variation.

Initially, the DCMG control starts at t = 0.05 s in the islanded mode with the condition that P_W is higher than P_L. In this case, the DCMG system operates in operating mode nine, in which the wind turbine unit works in the MPPT mode and the battery absorbs the surplus power of DCMG by regulating the DC-link voltage with $BVDM_{cha}$ according to the droop control in Figure 2a.

As the wind power is decreased at t = 0.35 s, the DC-link voltage V_{dc} is decreased from V_{nom}, which triggers the battery unit operation change from $BVDM_{cha}$ into $BVDM_{dis}$. Then, the resultant DCMG operation becomes the operating mode two.

As the battery SOC approaches to SOC_{min} at t = 0.51 s, the battery unit operation changes from $BVDM_{dis}$ into IDLE. Since the DCMG cannot supply the load due to a power deficit, the DC-link voltage continually decreases to V_{L2}. As soon as the DC-link voltage is reduced to V_{L2}, the load shedding algorithm starts, and the DCMG operating mode becomes one.

As a result of the load shedding process, the DC-link voltage gradually increases. In this figure, the transient response of the DC-link voltage is very slow after load shedding until 1.3 s. However, this is mainly caused by the fact that the surplus power within the DCMG system is very small during this duration. Eventually, when the DC-link voltage is sufficiently recovered above $V_{dc,B}^{ref}$, the battery unit operation changes from IDLE into $BVDM_{cha}$, resulting in the DCMG operating mode nine.

If the wind power generation P_W is quite increased at t = 1.5 s, the DC-link voltage V_{dc} increases beyond V_{nom}. Then, the wind power unit changes the operation from the MPPT mode into VDCM to reduce the generation power by the droop control. Once the

DC-link voltage becomes greater than V_{nom}, the load reconnecting algorithm reconnects the shed load.

The simulation result in Figure 8 clearly shows the dynamic variation of the DC-link voltage based on the voltage droop control in the islanded mode to ensure the power balance and load management in the decentralized DCMG system.

4.3. High Electricity Price Case

Figure 9 shows the simulation result of the proposed decentralized DCMG control scheme for a high electricity price condition. Initially, the DCMG system starts at t = 0.05 s with the operating mode seven in the grid-connected mode. With the decrease in P_W at t = 0.25 s, the DCMG operating mode is changed into six, in which the UG supplies the power deficit to the DCMG system with VCM_{con}.

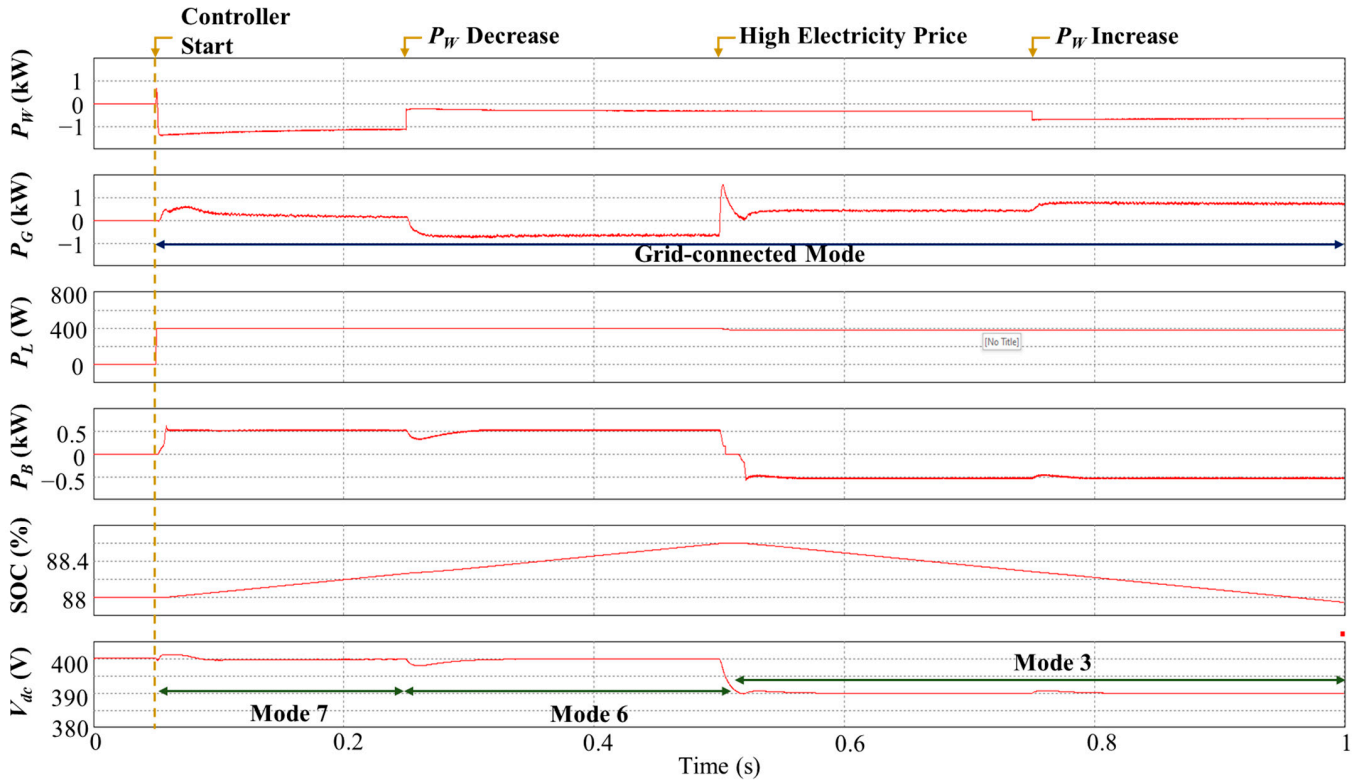

Figure 9. Simulation result in the case of a high electricity price.

When a high electricity price condition is detected at t = 0.5 s, the UG unit regulates the DC-link voltage V_{dc} to V_{L1}. With this value, the wind turbine unit operates in the MPPT mode and the battery unit in $BVDM_{dis}$, as shown in Figure 2b. The surplus power from the battery and wind turbine units is absorbed by the UG. To inject the power into the UG, the UG unit works in VCM_{inv} and the resultant DCMG operation becomes three. The main objective during a high electricity price condition is to minimize the electricity cost, which is achieved by minimizing the power supply by the UG, or by maximizing the power injection into the UG. Thus, even if the wind power generation is increased at t = 0.75 s, this DCMG operation is still maintained.

5. Experimental Results

To practically verify the overall control performance and effectiveness of the proposed PFCS for a decentralized DCMG system, the experiments were conducted using a prototype DCMG tested with the same configuration as in Figure 2. Figure 10 shows the configuration of the entire experimental DCMG system, which includes the power source, power electronics converters and controllers, DC-link capacitor, host PC to program the

controller, and oscilloscope for experimental waveform measurement. In the experiments, the AC motor control panel is used to drive an induction motor which is mechanically coupled to a PMSG to emulate a wind turbine unit. A bidirectional DC power source is employed as a battery, and the UG unit is connected to a three-phase grid through a transformer. The DC load unit is equipped with magnetic contactors for the implementation of load shedding and the reconnecting algorithm. Power converter controllers in each unit are realized by a 32-bit floating-point digital signal processor (DSP) TMS320F28335. Similar to the simulations, the experiments are also carried out for three cases: a high battery SOC case, low battery SOC case, and high electricity price case.

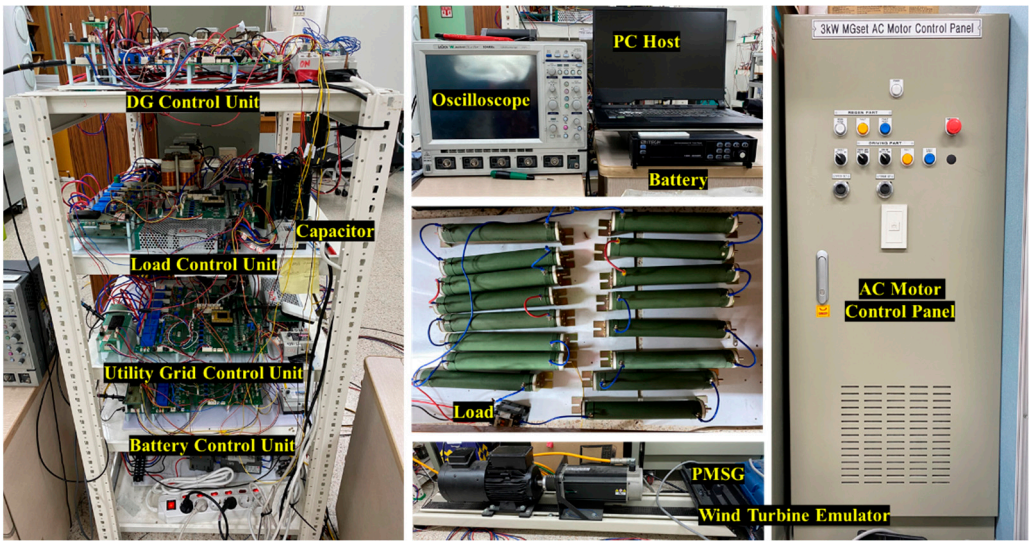

Figure 10. Configuration of the experimental DCMG system.

5.1. High Battery SOC Case

Figure 11 shows the experimental results of the proposed PFCS for a decentralized DCMG scheme when the battery is in the maximum SOC. Initially, the DCMG system operates at a steady-state with the operating mode six, as shown in Figure 11a with the load current, and Figure 11b with the wind power generation. In this condition, the DCMG system is in the grid-connected mode, and the wind turbine unit in the MPPT mode generates P_W more than P_L. However, since P_W is not sufficient for the maximum battery charging power P_B^{max}, this power deficit is provided by the UG unit with operation VCM_{con} to guarantee the system power balance. The UG unit regulates the DC-link voltage to the nominal value V_{nom}. The battery unit operates in $BVDM_{cha}$, and all loads are fed.

Figure 11c shows the transient responses of the DCMG system from the operating mode six into eight as the battery SOC reaches SOC_{max}. When the battery status reaches a fully charged condition, the battery unit operation is changed from $BVDM_{cha}$ to IDLE mode. Then, the power used to charge the battery is injected into the UG by changing the UG unit operation from VCM_{con} into VCM_{inv}. Even though the operation change of the UG unit introduces a transient response in the DC-link voltage regulation performance, it is stabilized quite fast, reaching the steady state. Figure 11d shows the steady-state responses after the operating mode transitions to eight, which shows a stable power balance in the DCMG system.

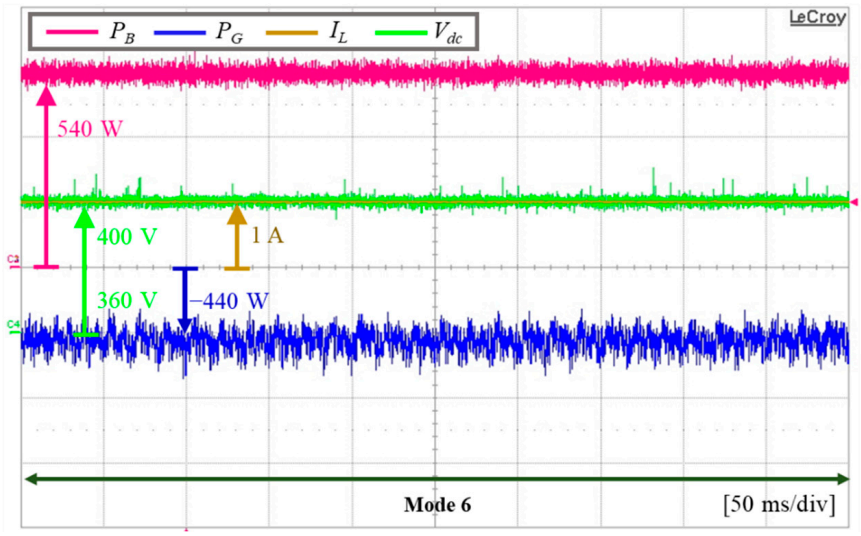

(**a**)

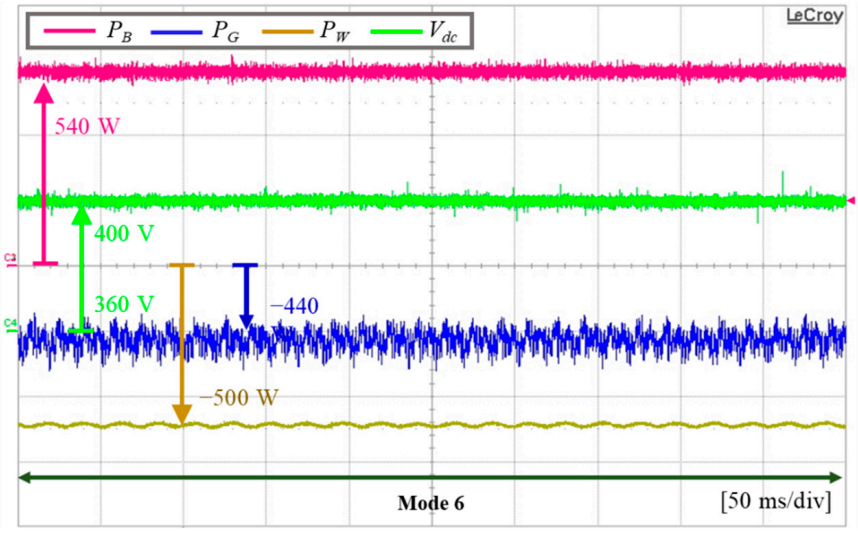

(**b**)

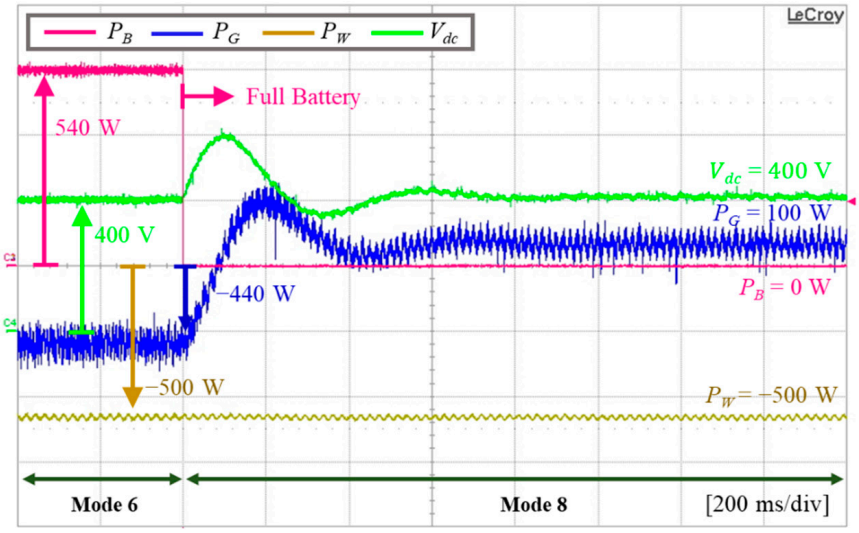

(**c**)

Figure 11. *Cont.*

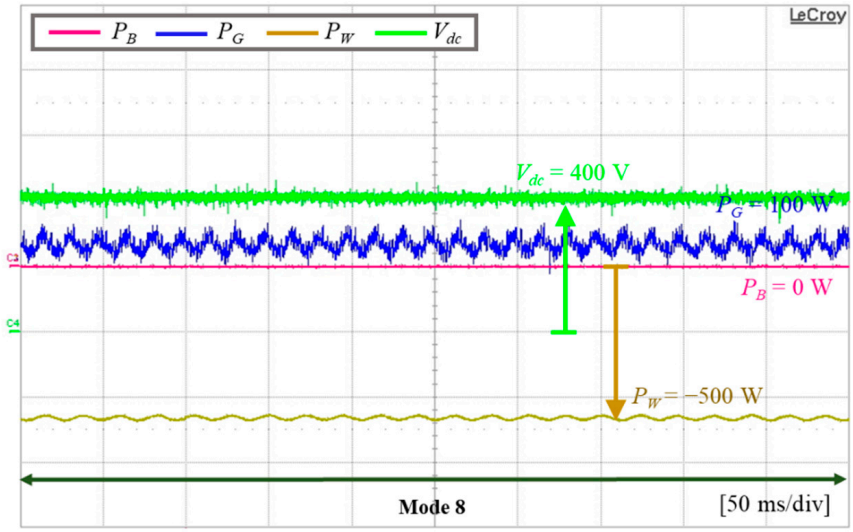

(**d**)

Figure 11. Experimental results of the proposed PFCS for a decentralized DCMG in grid-connected mode in the case of the maximum battery SOC. (**a**) Steady-state responses at operating mode 6 including I_L; (**b**) Steady-state responses at operating mode 6 including P_W; (**c**) Operating mode transition from mode 6 to 8; (**d**) Steady-state responses at operating mode 8.

5.2. Low Battery SOC Case

Figure 12 shows the experimental results of the proposed PFCS for a decentralized DCMG system when the UG has a fault. In this test, the DCMG system initially operates at a steady-state with the operating mode six in the condition of $P_W < P_L$, as shown in Figure 12a. The wind turbine and UG units supply 260 W and 680 W into the DC-link, which are absorbed by the battery unit and load. When the UG suddenly has a fault, as shown in Figure 12b, the DCMG operation is changed to the islanded mode. Since the power is not sufficient to supply the load, the proposed PFCS changes the operating mode from six to two. Before the transition, the UG regulates the DC-link voltage to V_{nom} (400 V) with operating mode six in the grid-connected mode. After the fault occurs in the UG, the battery unit supplies the power deficit into the DCMG system in the islanded mode by regulating the DC-link voltage with $BVDM_{dis}$ according to the voltage droop control characteristic in Figure 2a. In this test, the DC-link voltage decreases to 393 V after the transition. As a result, the wind turbine and battery units supply 386 W after the DCMG operation transition, which is absorbed by the load with a load power of $\frac{393^2}{400}$. The steady-state responses of the DCMG system after the mode transition into the islanded mode are shown in Figure 12c.

Figure 13 shows the experimental results in the islanded mode in the case of a low battery SOC and load shedding. Initially, the DCMG system is in operating mode two as shown in Figure 13a,b, in which the wind turbine and battery units provide 386 W into the DC-link at steady-state in MPPT mode and $BVDM_{dis}$, respectively.

Suddenly, as soon as the battery SOC reaches the SOC_{min} level, the battery operation changes from $BVDM_{dis}$ to IDLE mode. Figure 13c shows the DCMG operation transition for this case, in which the resultant DCMG operation is first changed from operating mode two to one. At this instant, the wind power P_W is insufficient to supply the load demand P_L and the DCMG system encounters the power deficit, causing the DC-link voltage to decrease. As soon as the DC-link voltage V_{dc} approaches V_{L2}, the load shedding algorithm starts to disconnect the load with the lowest priority, which can be observed during the mode one period in Figure 13c. As a result of the load shedding, the DC-link voltage gradually increases. When the DC-link voltage is increased to $V_{dc,B}^{ref}$, a second DCMG mode

transition occurs from the operating mode one to nine. In this operating mode, the battery unit works in $BVDM_{cha}$ to use the remaining power for charging.

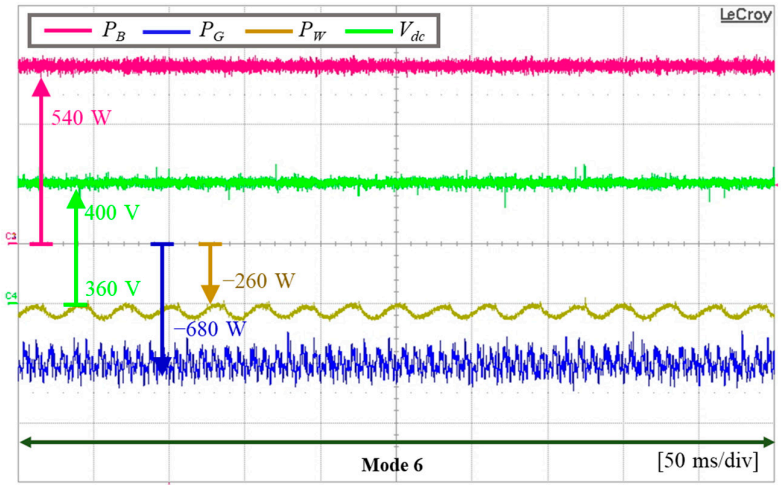

(**a**)

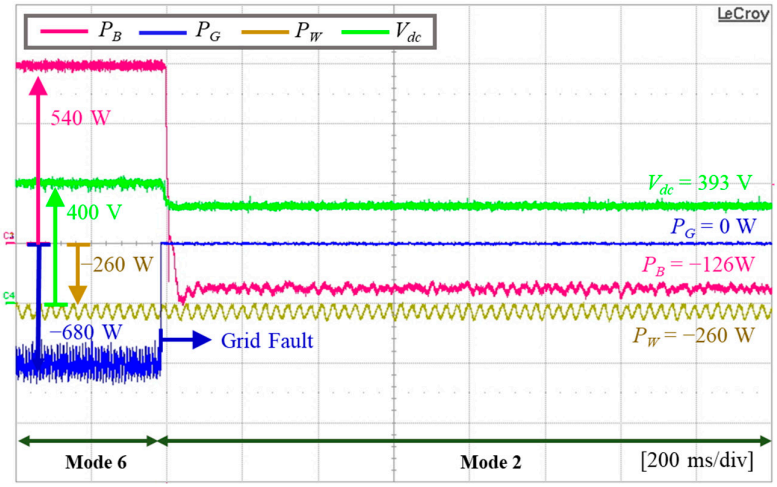

(**b**)

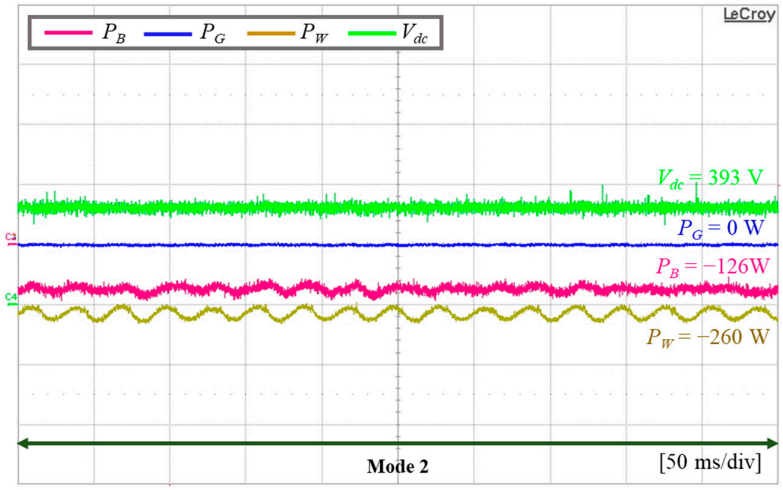

(**c**)

Figure 12. Experimental results of the proposed PFCS for a decentralized DCMG under grid fault with condition of $P_W < P_L$. (**a**) Steady-state responses at operating mode 6; (**b**) Operating mode transition from mode 6 to 2; (**c**) Steady-state responses at operating mode 2.

Figure 13d shows the steady-state responses of the DCMG system in operating mode nine. Although the DC-link voltage is varied in the islanded mode caused by the droop control characteristic in Figure 13, the proposed PFCS effectively achieves the power balance in a decentralized DCMG system.

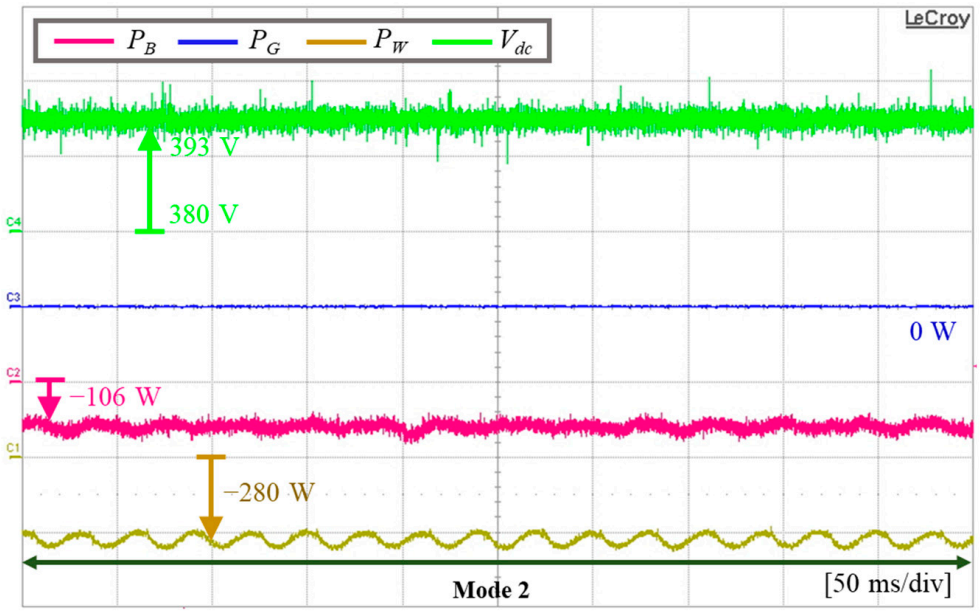

(**a**)

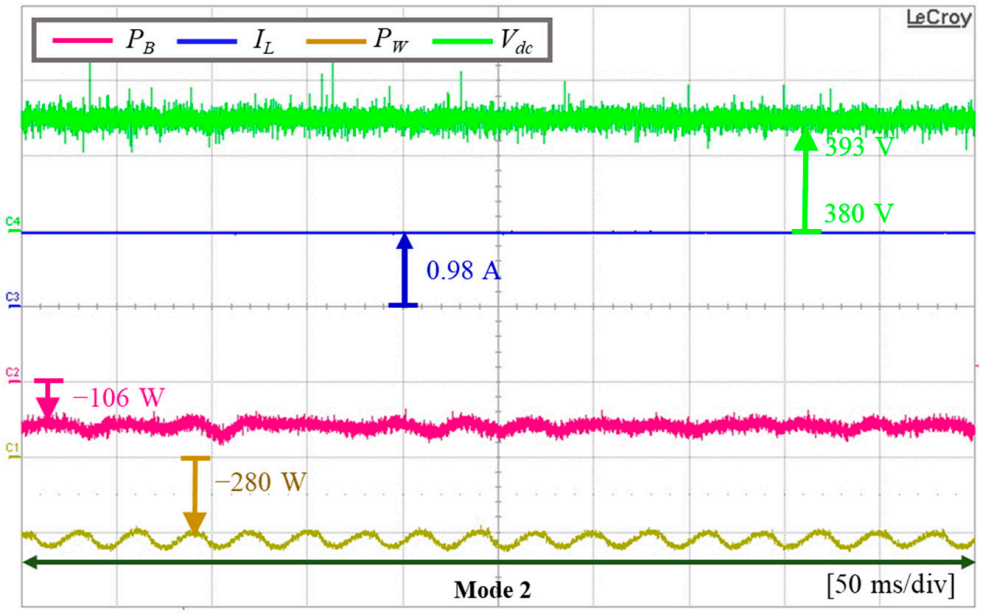

(**b**)

Figure 13. *Cont.*

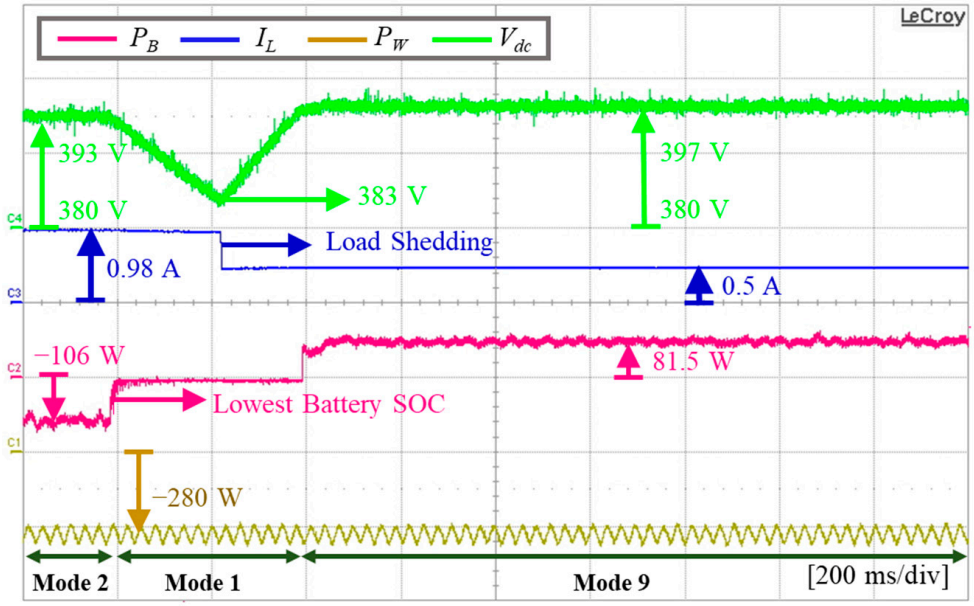

(**c**)

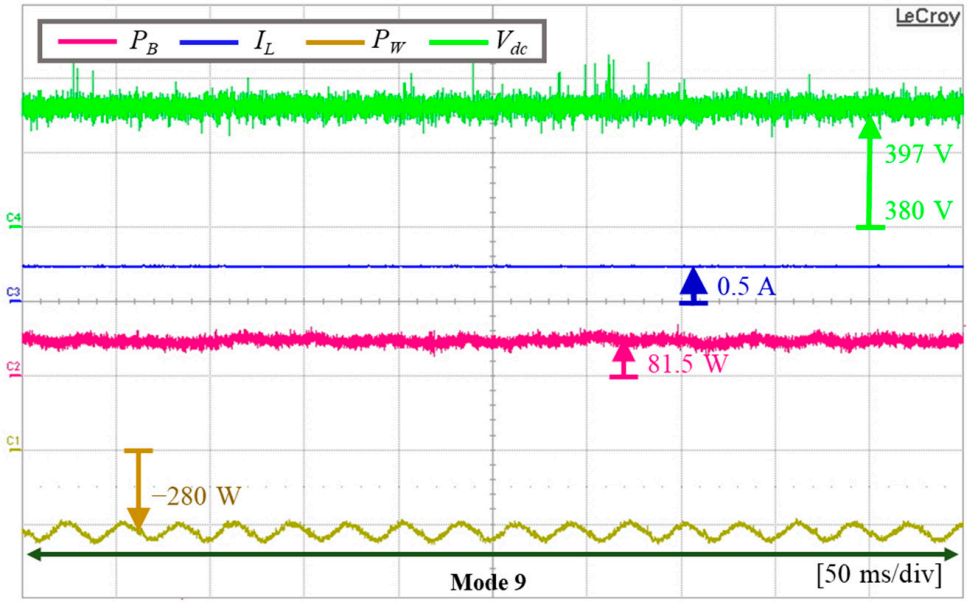

(**d**)

Figure 13. Experimental results of the proposed PFCS for a decentralized DCMG in islanded mode in the case of a low battery SOC and load shedding. (**a**) Steady-state responses at operating mode 2 including P_G; (**b**) Steady-state responses at operating mode 2 including I_L; (**c**) Operating mode transition from mode 2 to 1 and mode transition from 1 to 9; (**d**) Steady-state responses at operating mode 9.

5.3. High Electricity Price Case

Figure 14 shows the experimental results of the proposed PFCS for a decentralized DCMG system under a high electricity price case. Initially, the DCMG operation is the operating mode six at a steady-state, as shown in Figure 14a. In this condition, the wind power and UG units supply 940 W into the DC-link at a steady-state in MPPT mode and VCM_{con}, respectively, which is absorbed by the load and battery unit with $BVDM_{cha}$.

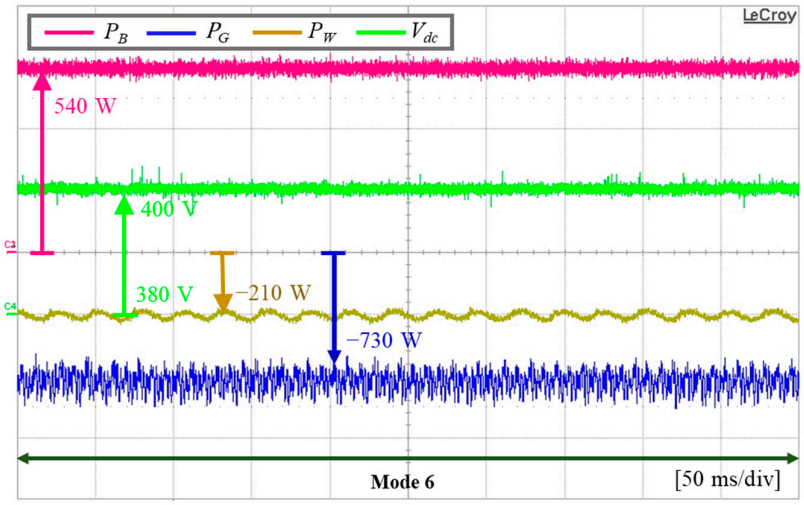

(**a**)

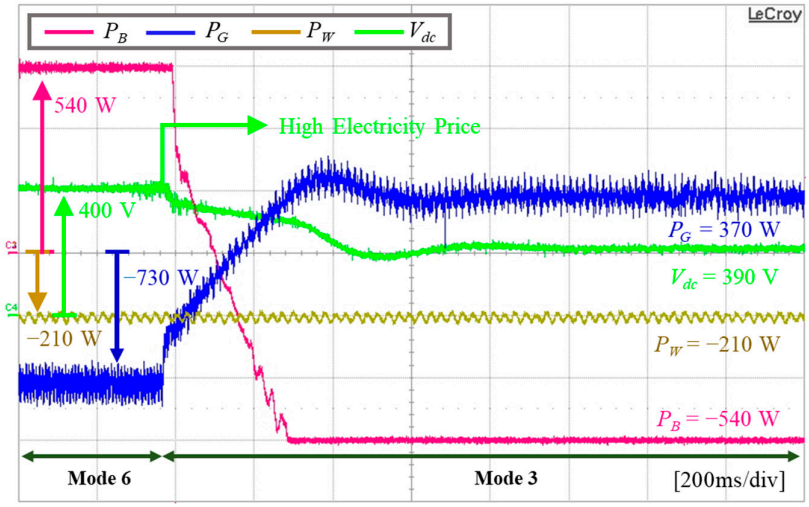

(**b**)

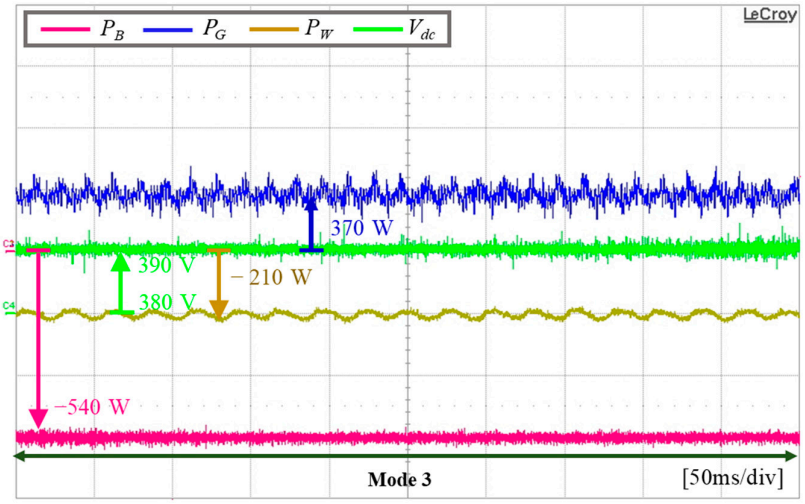

(**c**)

Figure 14. Experimental results of the proposed PFCS for a decentralized DCMG in grid-connected mode in the case of a high electricity price. (**a**) Steady-state responses at operating mode 6; (**b**) Operating mode transition from mode 6 to 3; (**c**) Steady-state responses at operating mode 3.

Once a high electricity price UG condition is detected, the DCMG mode transition occurs, as shown in Figure 14b, in which the proposed scheme changes the DCMG operating mode from six into three. In this condition, the UG unit changes the DC-link voltage reference from V_{nom} to V_{L1} to regulate V_{dc} to the V_{L1} level. With this value, the battery unit operates in $BVDM_{dis}$ instead of operating $BVDM_{con}$. This reduces the power usage from the UG and even injects the surplus power into the UG. Figure 14c shows the steady-state responses at operating mode three. In this mode, the wind turbine and battery units inject 750 W into the DC-link in MPPT mode and $BVDM_{dis}$, respectively, which is absorbed by the load and UG with VCM_{inv}.

6. Conclusions

To enhance the flexibility and scalability of the microgrid power system, this paper presented a PFCS for a decentralized DCMG system, which combines the voltage droop control and DC-link voltage control, with the consideration of the electricity price condition. By using the proposed scheme, each power unit autonomously decides its operating mode without additional communication links like the conventional decentralized control. To achieve power-sharing, the UG unit uses a DC-link voltage control in the grid-connected mode, while the DG and ESS units use the droop control method in the islanded mode. In the grid-connected mode, the DC-link voltage control method minimizes voltage deviation in the DCMG system. The droop control method utilized in the wind turbine and battery units achieves the power balance without additional communication links. The presented droop control method can work correctly with the DC-link voltage controller to achieve power-sharing in several conditions presented in the PFCS. Furthermore, the proposed PFCS adaptively changes the DC-link voltage level according to electricity price conditions to minimize the utility cost. The main contributions of this paper can be summarized as follows:

(i) The proposed decentralized DCMG system can achieve power-sharing and energy management among power units without additional communication links. In the grid-connected mode, power-sharing and energy management are ensured by the UG, considering the electricity price condition. On the contrary, in the islanded mode, they are achieved by the DG, ESS, and load units according to the wind power, battery SOC, and load demand condition.

(ii) A PFCS for a decentralized DCMG architecture that combines voltage droop control and DC-link voltage control is proposed. The proposed PFCS, consisting of eleven operating modes, enhances the DCMG system reliability in the presence of uncertainties such as the wind power variation, battery SOC level, load demand, and grid availability.

(iii) Depending on the electricity price condition, the proposed PFCS adaptively changes the DC-link voltage level in the grid-connected mode to minimize the utility cost without affecting the DCMG system operation stability. Hence, by reducing the DC-link voltage level during a high electricity price condition, the UG supports only the required minimum power to the DCMG, or, conversely, the UG absorbs the maximum power available from the DCMG.

The proposed PFCS for a decentralized DCMG system has been validated by both the simulations based on the PSIM software and the experiments based on a laboratory DCMG testbed. Comprehensive simulation and experimental results under various test conditions demonstrate the effectiveness and usefulness of the proposed power flow control scheme. The voltage droop control and DC-link voltage control are combined well, and thus, the power flow control of a decentralized DCMG is quite stable during the mode transition between the grid-connected mode and islanded mode. Test results also confirm the control flexibility and overall performance of the proposed scheme even under several existing uncertainties.

Author Contributions: A.F.H., F.A.P. and K.-H.K. conceived the main concept of the microgrid control structure and developed the entire system; A.F.H. carried out the research and analyzed the numerical data with guidance from K.-H.K.; A.F.H., F.A.P. and K.-H.K. collaborated in the preparation of the manuscript. All authors have read and agreed to the published version of the manuscript.

Funding: This research was supported by Basic Science Research Program through the National Research Foundation of Korea (NRF) funded by the Ministry of Education (NRF-2019R1A6A1A03032119). This work was supported by the National Research Foundation of Korea (NRF) grant funded by the Korea government (MSIT) (NRF-2020R1F1A1048262).

Institutional Review Board Statement: Not applicable.

Informed Consent Statement: Not applicable.

Data Availability Statement: Data sharing is not applicable to this article.

Acknowledgments: This research was supported by Basic Science Research Program through the National Research Foundation of Korea (NRF) funded by the Ministry of Education (NRF-2019R1A6A1A03032119). This work was supported by the National Research Foundation of Korea (NRF) grant funded by the Korea government (MSIT) (NRF-2020R1F1A1048262).

Conflicts of Interest: The authors declare no conflict of interest.

Abbreviations

AC	Alternating current
ACMG	AC microgrid
DC	Direct current
DCMG	DC microgrid
DCLs	Digital communication links
DG	Distributed generation
DSP	Digital signal processor
ESS	Energy storage system
IDLE	Idle mode by battery unit
MPPT	Maximum power point tracking
PCC	Point of common coupling
PFCS	Power flow control strategy
PI	Proportional integral
PLL	Phase lock loop
PMSG	Permanent magnet synchronous generator
PSIM	Power simulation software
PWM	Pulse width modulation
PV	Photovoltaic
RES	Renewable energy source
RTP	Real-time price
SOC	State of charge
SPT	Stepwise power tariff
SHED	Load shedding
SVPWM	Space vector pulse width modulation
TOU	Time of use pricing
UG	Utility grid
VDCM	Voltage droop control mode by wind turbine unit
$BVDM_{cha}$	Battery voltage droop control by charging mode
$BVDM_{dis}$	Battery voltage droop control by discharging mode
C_{dc}	Capacitance of DC-link
C_f	Filter capacitance of LCL filter
f_G	Grid frequency
I_B	Battery current
I_B^{ref}	Battery curren reference

$I_{q,G}$	*q-axis* utility grid current
$I_{q,W}$	*q-axis* wind turbine current
$I_{q,G}^{ref}$	*q-axis* utility grid current reference
$I_{q,W}^{ref}$	*q-axis* wind turbine current reference
J	PMSG inertia
L_B	Converter filter inductance of battery unit
L_{dq}	PMSG *dq*-axis inductance
L_W	Converter filter inductance of wind power unit
L_1	Inverter-side inductance of LCL filter
L_2	Grid-side inductance of LCL filter
P_B	Exchanged power between DC-link and battery unit
P_B^{max}	Maximum power charging (+)/discharging (−) of battery unit
P_G	Exchanged power between DC-link and utility grid unit
P_L	Power absorbed by load unit
P_{L1}	Power of load 1
P_{L2}	Power of load 2
P_W	Generation power by wind power unit
P_W^{max}	Maximum release (−) power of wind power unit
Pr	Electricity price
Pr_{high}	High electricity price condition
Pr_{low}	Low electricity price condition
$R_{droop,B}$	Droop characteristic of battery unit
$R_{droop,W}$	Droop characteristic of wind turbine unit
R_s	PMSG stator resistance
R_W	L filter resistances of wind power unit
R_1	Parasitic resistance in L_1
R_2	Parasitic resistance in L_2
SOC_{max}	Maximum SOC
SOC_{min}	Minimum SOC
V_B	Battery voltage
V_B^{max}	Maximum battery voltage
V_H	DC-link maximum voltage
V_G^{rms}	Grid voltage
V_{L1}	DC-link Level 1 minimum voltage
V_{L2}	DC-link Level 2 minimum voltage
$V_{abc,G}$	Grid voltages in synchronous reference frame
$V_{abc,G}$	Wind turbine voltages in synchronous reference frame
$V_{d,G}^{ref}$	*d-axis* utility grid voltage reference
$V_{d,W}^{ref}$	*d-axis* wind turbine voltage reference
V_{dc}	DC-link voltage
$V_{dc,B}^{ref}$	DC-link voltage reference of battery unit
$V_{dc,G}^{ref}$	DC-link voltage reference of utility grid unit
$V_{dc,W}^{ref}$	DC-link voltage reference of wind turbine unit
V_{nom}	DC-link nominal voltage
VCM_{con}	DC-link voltage control by converter mode
VCM_{inv}	DC-link voltage control by inverter mode
ψ	PMSG flux linkage

References

1. Huang, B.B.; Xie, G.H.; Kong, W.Z.; Li, Q.H. Study on Smart Grid and Key Technology System to Promote the Development of Distributed Generation. In Proceedings of the IEEE PES Innovative Smart Grid Technologies, Tianjin, China, 21–24 May 2012; pp. 1–4.
2. Ensermu, G.; Bhattacharya, A.; Panigrahy, N. Real-Time Simulation of Smart DC Microgrid with Decentralized Control System under Source Disturbances. *Arab. J. Sci. Eng.* **2019**, *44*, 7173–7185. [CrossRef]
3. Adhikari, S.; Xu, Q.; Tang, Y.; Wang, P.; Li, X. Decentralized Control of Two DC Microgrids Interconnected with Tie-Line. *J. Mod. Power Syst. Clean Energy* **2017**, *5*, 599–608. [CrossRef]

4. Ansari, S.; Chandel, A.; Tariq, M. A Comprehensive Review on Power Converters Control and Control Strategies of AC/DC Microgrid. *IEEE Access* **2020**, *9*, 17998–18015. [CrossRef]
5. Carpintero-Rentería, M.; Santos-Martín, D.; Guerrero, J.M. Microgrids Literature Review through a Layers Structure. *Energies* **2019**, *12*, 4381. [CrossRef]
6. Al-Ismail, F.S. DC Microgrid Planning, Operation, and Control: A Comprehensive Review. *IEEE Access* **2021**, *9*, 36154–36172. [CrossRef]
7. Dragičević, T.; Lu, X.; Vasquez, J.C.; Guerrero, J.M. DC Microgrids—Part II: A Review of Power Architectures, Applications, and Standardization Issues. *IEEE Trans. Power Electron.* **2016**, *31*, 3528–3549. [CrossRef]
8. Dai, Y.; Gao, Y.; Gao, H.; Zhu, H. Real-time Pricing Scheme Based on Stackelberg Game in Smart Grid with Multiple Power Retailers. *Neurocomputing* **2017**, *260*, 149–156. [CrossRef]
9. Zhou, L.; Zhang, Y.; Lin, X.; Li, C.; Cai, Z.; Yang, P. Optimal Sizing of PV and BESS for A Smart Household Considering Different Price Mechanisms. *IEEE Access* **2018**, *6*, 41050–41059. [CrossRef]
10. Zhou, B.; Yang, R.; Li, C.; Cao, Y.; Wang, Q. Multiobjective Model of Time-of-use and Stepwise Power Tariff for Residential Consumer in Regulated Power Markets. *IEEE Syst. J.* **2018**, *12*, 2676–2687. [CrossRef]
11. Wang, H.; Fang, H.; Yu, X.; Liang, S. How Real Time Pricing Modifies Chinese Households' Electricity Consumption. *J. Clean. Prod.* **2018**, *178*, 776–790. [CrossRef]
12. Renfang, L.; Luping, S.; Sidai, G. The Stepwise Pricing Mechanism Research of Residents' Living Power. *Energy Procedia* **2011**, *5*, 1371–1376. [CrossRef]
13. Gao, F.; Kang, R.; Cao, J.; Yang, T. Primary and Secondary Control in DC Microgrids: A Review. *J. Mod. Power Syst. Clean Energy* **2019**, *7*, 227–242. [CrossRef]
14. Mehdi, M.; Kim, C.H.; Saad, M. Robust Centralized Control for DC Islanded Microgrid Considering Communication Network Delay. *IEEE Access* **2020**, *8*, 77765–77778. [CrossRef]
15. Padhilah, F.A.; Kim, K.-H. A Power Flow Control Strategy for Hybrid Control Architecture of DC Microgrid under Unreliable Grid Connection Considering Electricity Price Constraint. *Sustainability* **2020**, *12*, 7628. [CrossRef]
16. Espina, E.; Llanos, J.; Burgos-Mellado, C.; Cárdenas-Dobson, R.; Martínez-Gómez, M.; Sáez, D. Distributed Control Strategies for Microgrids: An Overview. *IEEE Access* **2020**, *8*, 193412–193448. [CrossRef]
17. Tuckey, A.; Zabihi, S.; Round, S. Decentralized Control of A Microgrid. In Proceedings of the 2017 19th European Conference on Power Electronics and Applications (EPE'17 ECCE Europe), Warsaw, Poland, 11–14 September 2017.
18. Peyghami-Akhuleh, S.; Mokhtari, H.; Davari, P.; Loh, P.C.; Blaabjerg, F. Smart Power Management of DC Microgrids in Future Milligrids. In Proceedings of the 2016 18th European Conference on Power Electronics and Applications (EPE'16 ECCE Europe), Karlsruhe, Germany, 5–9 September 2016; pp. 1–10.
19. Khorsandi, A.; Ashourloo, M.; Mokhtari, H. A Decentralized Control Method for a Low-Voltage DC Microgrid. *IEEE Trans. Energy Convers.* **2014**, *29*, 793–801. [CrossRef]
20. Xu, Q.; Xiao, J.; Hu, X.; Wang, P.; Lee, M.Y. A Decentralized Power Management Strategy for Hybrid Energy Storage System with Autonomous Bus Voltage Restoration and State-of-Charge Recovery. *IEEE Trans. Ind. Electron.* **2017**, *64*, 7098–7108. [CrossRef]
21. Guerrero, J.M.; Vasquez, J.C.; Matas, J.; De Vicuña, L.G.; Castilla, M. Hierarchical Control of Droop-Controlled AC and DC Microgrids—A General Approach toward Standardization. *IEEE Trans. Ind. Electron.* **2010**, *58*, 158–172. [CrossRef]
22. Gao, F.; Bozhko, S.; Costabeber, A.; Patel, C.; Wheeler, P.; Hill, C.I.; Asher, G. Comparative Stability Analysis of Droop Control Approaches in Voltage-Source-Converter-Based DC Microgrids. *IEEE Trans. Power Electron.* **2016**, *32*, 2395–2415. [CrossRef]
23. Gu, Y.; Xiang, X.; Li, W.; He, X. Mode-Adaptive Decentralized Control for Renewable DC Microgrid with Enhanced Reliability and Flexibility. *IEEE Trans. Power Electron.* **2014**, *29*, 5072–5080. [CrossRef]
24. Han, Y.; Yang, H.; Li, Q.; Chen, W.; Zare, F.; Guerrero, J.M. Mode-Triggered Droop Method for The Decentralized Energy Management of An Islanded Hybrid PV/Hydrogen/Battery DC Microgrid. *Energy* **2020**, *199*, 117441. [CrossRef]
25. Gao, L.; Liu, Y.; Ren, H.; Guerrero, J.M. A DC Microgrid Coordinated Control Strategy Based on Integrator Current-Sharing. *Energies* **2017**, *10*, 1116. [CrossRef]
26. Merai, M.; Naouar, M.W.; Slama-Belkhodja, I.; Monmasson, E. An Adaptive PI Controller Design for DC-Link Voltage Control of Single-Phase Grid-Connected Converters. *IEEE Trans. Ind. Electron.* **2018**, *66*, 6241–6249. [CrossRef]
27. Nguyen, T.V.; Kim, K.-H. Power Flow Control Strategy and Reliable DC-Link Voltage Restoration for DC Microgrid under Grid Fault Conditions. *Sustainability* **2019**, *11*, 3781. [CrossRef]
28. Nguyen, T.V.; Kim, K.-H. An Improved Power Management Strategy for MAS-Based Distributed Control of DC Microgrid under Communication Network Problems. *Sustainability* **2020**, *12*, 122. [CrossRef]